

The discovery of a nearby 421 s transient with CHIME/FRB/Pulsar

Fengqiu Adam Dong^{1*}, Tracy Clarke², Alice P. Curtin^{3,4},
Ajay Kumar⁵, Ingrid Stairs¹, Shami Chatterjee⁶,
Amanda M. Cook^{7,8}, Emmanuel Fonseca^{9,10}, B. M. Gaensler^{8,11},
Jason W.T. Hessels^{3,4,12,13}, Victoria M. Kaspi^{3,4}, Mattias Lazda^{7,8},
Kiyoshi W. Masui^{14,15}, James W. McKee^{16,17},
Bradley W. Meyers¹⁸, Aaron B. Pearlman^{3,4}, Scott M. Ransom¹⁹,
Paul Scholz^{8,20}, Kaitlyn Shin^{14,15}, Kendrick M. Smith²¹,
Chia Min Tan¹⁸

^{1*}Department of Physics & Astronomy, University of British Columbia,
325 - 6224 Agricultural Road, Vancouver, V6T 1Z1, British Columbia,
Canada.

²U.S. Naval Research Laboratory, 4555 Overlook Ave, SW Washington,
20375, DC, USA.

³Department of Physics, McGill University, 3600 rue University,
Montréal, H3A 2T8, QC, Canada.

⁴Trottier Space Institute, McGill University, 3600 rue University,
Montréal, H3A 2A7, QC, Canada.

⁵Tata Institute of Fundamental Research, National Centre for Radio
Astronomy, Savitribai Phule Pune University Campus Spicer College
Road, Ganeshkhind, Pune, HR6G+3G5, 411007, Maharashtra, India.

⁶Cornell Center for Astrophysics and Planetary Science, Cornell
University, , Ithaca, 14853, NY, USA.

⁷David A. Dunlap Department of Astronomy & Astrophysics, University
of Toronto, 50 St. George Street, Toronto, M5S 3H4, Ontario, Canada.

⁸Dunlap Institute for Astronomy & Astrophysics, University of Toronto,
50 St. George Street, Toronto, M5S 3H4, Ontario, Canada.

⁹Department of Physics and Astronomy, West Virginia University, ,
Morgantown, 26506-6315, WV, USA.

- ¹⁰Center for Gravitational Waves and Cosmology, West Virginia University, Chestnut Ridge Research Building, Morgantown, 26505, WV, USA.
- ¹¹University of California Santa Cruz, 1156 High St, Santa Cruz, 95064, CA, USA.
- ¹²ASTRON, Netherlands Institute for Radio Astronomy, Oude Hoogeveensedijk 4, Dwingeloo, PD, 7991, The Netherlands.
- ¹³Anton Pannekoek Institute for Astronomy, University of Amsterdam, Science Park 904, Amsterdam, 1098, XH, The Netherlands.
- ¹⁴Department of Physics, Massachusetts Institute of Technology, 77 Massachusetts Ave, Cambridge, 02139, MA, USA.
- ¹⁵MIT Kavli Institute for Astrophysics and Space Research, Massachusetts Institute of Technology, 77 Massachusetts Ave, McNair Building (MIT Building 37), Cambridge, 02139, MA, USA.
- ¹⁶E.A. Milne Centre for Astrophysics, University of Hull, Cottingham Road, Kingston-upon-Hull, HU6 7RX, UK.
- ¹⁷Centre of Excellence for Data Science Artificial Intelligence and Modelling (DAIM), University of Hull, Cottingham Road, Kingston-upon-Hull, HU6 7RX, UK.
- ¹⁸International Centre for Radio Astronomy Research, Curtin University, Bentley, 6102, WA, Australia.
- ¹⁹National Radio Astronomy Observatory, 520 Edgemont Road, Charlottesville, 22903, VA, USA.
- ²⁰York University, 4700 Keele Street, Toronto, M3J 1P3, ON, Canada.
- ²¹Perimeter Institute for Theoretical Physics, 31 Caroline St N, Waterloo, N2L 2Y5, ON, Canada.

*Corresponding author(s). E-mail(s): fengqiu.dong@gmail.com;

Abstract

Neutron stars and white dwarfs are both dense remnants of post-main-sequence stars. Pulsars, magnetars and strongly magnetised white dwarfs have all been seen to be observed to exhibit coherent, pulsed radio emission in relation to their rotational period. Recently, a new type of radio long period transient (LPT) has been discovered. The bright radio emission of LPTs resembles that of radio pulsars and magnetars. However, they pulse on timescales (minutes) much longer than previously seen. While minute timescales are common rotation periods for white dwarfs, LPTs are much brighter than the known pulsating white dwarfs, and dipolar radiation from isolated (as opposed to binary) magnetic white dwarfs has yet to be observed. Here, we report the discovery of a new ~ 421 s LPT, CHIME J0630+25, using the CHIME/FRB and CHIME/Pulsar instruments. We

used standard pulsar timing techniques and obtained a phase-coherent timing solution which yielded limits on the inferred magnetic field and characteristic age. CHIME J0630+25 is remarkably nearby (170 ± 80 pc), making it the closest LPT discovered to date.

Keywords: keyword1, Keyword2, Keyword3, Keyword4

Recently, a new class of objects known as radio long-period transients (LPTs)¹ has been discovered. Four such objects have been confirmed: GLEAM-X J162759.5–523504.3 [1] and GPM 1839–10 [2], both discovered by the Murchison Widefield Array (MWA), ASKAP J1935+2148 [3], discovered by the Australian Square Kilometre Array Pathfinder (ASKAP) telescope, and PSR J0901–4046 [4], discovered by the MeerKAT telescope (1091 s for GLEAM-X J162759.5–523504.3, 1318 s for GPM 1839–10, 3225 s for ASKAP J1935+2148, and 76 s for PSR J0901–4046). However, their nature remains mysterious.

These LPTs are characterised by their exceptionally long periods, wide burst widths (up to 60 seconds), and complex temporal and spectral microstructure. Two types of sources, white dwarfs and neutron stars, have emerged as the favoured models for LPTs due to their emission characteristics and rotation periods.

Radio pulsars are the most common form of detectable neutron star. They are remarkably accurate celestial clocks. By carefully measuring pulse times of arrival (TOAs), we can fully account for every rotation of a pulsar through a process called pulsar timing. The rotational period and period derivative obtained via pulsar timing provide critical constraints [5, 6] on the mechanisms of coherent radio emission [7–9]. The constraints derived from pulsar timing assume that the emissions are powered by rotational energy loss. However, not all emission from neutron stars is powered by spin-down. A subset of magnetically-powered young neutron stars, namely magnetars, exhibits noisy rotational behaviour and drastically changing pulse-to-pulse emissions punctuated by high-energy outbursts [see 10, 11, for reviews]. Accomplishing phase-coherent timing for magnetars can be challenging due to their apparent rotational instability that often but not exclusively occurs contemporaneously with X-ray outbursts [e.g. 12, 13]. The complex temporal and spectral structure of LPT radio emission is somewhat similar to that of magnetars, and some have argued [14] that this favours a neutron-star model for LPTs [15, 16]. However, radio emission from neutron stars with periods as long as those of LPTs has not yet been observed. The longest period pulsar, PSR J0250+5854, has a rotational period of 23.5 s [17]. There is one magnetar candidate, 1E 161348-5055, with a period of 6.67 h at the centre of supernova remnant RCW103 [18]. However, only high-energy emission has ever been detected from 1E 161348-5055 [19, 20].

White dwarfs are an alternative explanation for LPTs due to their longer rotational periods. Most white dwarf emission is not periodic or detectable in radio [21].

¹Note that these sources have also been given some other names in the literature such as ultra long period transients (ULPT), long period radio transients (LPRT). In this study, we use the term long period transient throughout.

However, recently two white dwarfs have been discovered to emit pulsed emission in the radio band like pulsars, AR Scorpii and J1912–4410 [22, 23]. In the case of J1912–4410, the emission was detectable down to 1.4 GHz with duty cycles similar to radio pulsars. Additionally, the periods of the white dwarfs producing coherent pulsed radio emissions are similar to those of the discovered LPTs. Yet, a couple of issues remain with the white dwarf model for LPTs. Despite optical searches, no optical counterparts have been identified in the localisation regions of any LPT [4]. In addition, only white dwarfs in binary systems have been seen to emit coherent radio emission. At least one LPT, PSR J0901–4046, has well-constrained timing parameters, which show it to be an isolated source. While it is theoretically possible for an isolated white dwarf to produce coherent radio pulses, this has yet to be observed.

We have discovered a new $P = 421.35542$ s LPT using the Canadian Hydrogen Intensity Mapping Experiment (CHIME) telescope, CHIME J0630+25, utilising search strategies developed for Galactic pulsar searches [24]. We have also obtained a phase-coherent timing solution for CHIME J0630+25. The discovery marks the closest LPT to date at 170(80) pc. Additionally, we have identified two potential X-ray counterparts to CHIME J0630+25 using the *Neil Gehrels Swift* telescope, although the radio localisation region is large.

Results

CHIME, located near Penticton, British Columbia, Canada, is a transit telescope comprised of four cylindrical dishes and three distinct backend instruments: CHIME/-Cosmology [25], CHIME/FRB [26], and CHIME/Pulsar [27]. The unique cylindrical design of CHIME offers a wide field of view (FOV) of approximately 200 square degrees at any given time. Additionally, as an interferometric telescope, CHIME/FRB can form 1024 static synthesised beams within its large primary beam, allowing for the localisation of astrophysical transients with a typical precision of ~ 0.5 degrees. The extensive FOV enables CHIME/FRB to survey the entire northern sky daily. Of particular interest is CHIME/FRB’s capability to perform continuous single pulse surveys, enabling the detection of even highly sporadic sources, including repeating and one-off FRBs [28], rotating radio transients [24], and LPTs. We identified an astrophysical candidate with the first detection occurring on MJD 58772 at 12:54:51 UTC (see Methods) at Right Ascension (RA) $06:30:43 \pm 6''$, Declination (Dec) $25:23:24 \pm 11''$ where the quoted uncertainty is at the 1σ level.² This candidate, CHIME J0630+25, was then followed up by the more sensitive CHIME/Pulsar instrument with 688 observations, totalling ~ 176 hours between MJDs 59300 and 60116. These are in the form of high-time resolution Stokes-I spectra. We detected 11 bursts with the CHIME/Pulsar observations. We also detected 6 bursts with CHIME/FRB. The CHIME/FRB detections only had metadata recorded. However, we confirmed that these bursts are indeed from CHIME J0630+25, as they are consistent with its rotation period. Additionally, one of the bursts was a co-detection with both backends. All the detections are provided in Table 1, which includes the fluence, effective width, spectral index, and burst

²All coordinates in this study are given in the J2000 coordinate system.

Table 1: Properties for the pulses for CHIME J0630+25 detected by the CHIME/FRB and CHIME/Pulsar systems. For the CHIME/FRB detections, we report the TOA in UTC time at CHIME referenced to 400 MHz, signal-to-noise ratio (S/N), and the automated pipeline DM. For the CHIME/Pulsar detections, we report the pulse TOAs referenced to 800 MHz and provide calibrated characteristics from the total intensity data stream. This includes the effective width (W_{eff}), fluence (F), spectral index (α), DM, and a burst category that facilitates the quasiperiodicity analysis described further in the Methods. The CHIME/FRB detections lack W_{eff} , F , α and Burst Category values as Stokes-I intensity data do not exist for these bursts. This is discussed in more detail in the main text. Note that we omit the detection S/N of the pulses detected by CHIME/Pulsar as the detection pipeline is different from CHIME/FRB, and the detection S/N is not directly comparable. Therefore, to avoid confusion, we only provide the fluence.

Burst	Instrument	TOA MJD	W_{eff} ms	F Jy ms	α	DM pc cm $^{-3}$	Burst Category	Detection S/N
58772A	CHIME/FRB	58772.53808(1)	–	–	–	23(3)	–	12.9
58855A	CHIME/FRB	58855.30794(1)	–	–	–	23(3)	–	9.7
58860A	CHIME/FRB	58860.29698(1)	–	–	–	24(3)	–	15.0
58871A	CHIME/FRB	58871.26526(1)	–	–	–	24(3)	–	9.4
59167A	CHIME/FRB	59167.45383(1)	–	–	–	24(3)	–	10.7
59553A*	CHIME/FRB	59553.39770(1)	–	–	–	23(3)	–	8.7
59341A	CHIME/Pulsar	59341.97314(2)	770(230)	270(80)	-1.8(3)	20(3)	C1	–
59341B	CHIME/Pulsar	59341.97803(1)	280(90)	90(30)	-1.5(3)	23(3)	C1	–
59456A	CHIME/Pulsar	59456.65990(1)	320(100)	90(30)	-2.7(3)	23(3)	C1	–
59456B	CHIME/Pulsar	59456.66474(1)	400(120)	90(30)	-2.0(3)	23(3)	C1	–
59460A	CHIME/Pulsar	59460.64875(1)	280(90)	310(90)	-2.1(3)	20(3)	C3	–
59463A	CHIME/Pulsar	59463.64282(2)	910(270)	670(200)	-2.1(3)	22(6)	C3	–
59548A	CHIME/Pulsar	59548.41384(1)	470(140)	200(60)	-2.2(3)	20(3)	C1	–
59553A*	CHIME/Pulsar	59553.39770(1)	470(140)	550(160)	-2.3(3)	20(7)	C2	–
59563A	CHIME/Pulsar	59563.37042(2)	650(200)	500(150)	-2.5(3)	23(3)	C2	–
59565A	CHIME/Pulsar	59565.36500(1)	180(60)	90(30)	-1.2(3)	21(3)	C1	–
59574A	CHIME/Pulsar	59574.34304(2)	200(60)	60(20)	-1.9(3)	25(4)	C2	–

* This pulse was simultaneously detected with both the CHIME/Pulsar and CHIME/FRB systems. We report the measurement from each instrument separately.

category for each burst (see Methods). The burst category is a classification system that we used for the quasiperiodicity analysis described in the Methods section.

The dynamic spectra for the CHIME/Pulsar detections are shown in Figure 1 and show a more complex temporal and spectral structure than in conventional radio pulsars. The bursts can span widths up to ~ 4 s (1% of the period, in the case of 59463A) and can show erratic sub-structures reminiscent of the radio bursts seen from radio-loud magnetar XTE 1910–197 [15, 16] (in the case of 59460A).

An initial periodicity analysis was performed with the `rrat_period` package from PRESTO³. `rrat_period` works by iterating over many different trial periods to find the period most likely to be an integer factor of the spacing between successive bursts. Using barycentre corrected arrival times with `rrat_period` yielded $P \approx 421$ s. This was then refined using TEMPO2 [29] and PINT [30] to obtain a phase-coherent timing solution with period of $P = 421.35542(1)$ s and $\dot{P} = -2.5(1.6) \times 10^{-12}$ ss $^{-1}$ at $1\text{-}\sigma$

³<https://github.com/scottransom/presto>

uncertainty (see Methods). The full set of phase-coherent timing parameters is given in Table 2. As a result of the low numbers of TOAs and the large uncertainties on each TOA, we emphasise that the negative \dot{P} could contain significant covariances with position. To date, most pulsars which are spinning up have been found in binaries [e.g. 31]. Therefore, if the negative \dot{P} were to be believed, then CHIME J0630+25 likely exists in a tight binary like the AR Scorpii and J1912–4410 systems. This is given further analysis in the Discussion section. More detections are required to determine \dot{P} robustly. Consequently, we adopted a 1- σ shifted upper limit on \dot{P} as discussed below.

Dispersion measure (DM) is a frequency dependent delay from the ionized component of the interstellar medium. This affects all radio pulses from pulsars and white dwarfs. The DM allows us to estimate the distance to the source using interstellar medium models. There exist two models for the Galactic electron density, NE2001 [32] and YMW16 [33]. We estimate the distance to CHIME J0630+25 using the YMW16 Galactic electron density model [33]. Analyses of Galactic interstellar medium models have shown that the YMW16 model is better than the NE2001 electron density model [32] for nearby pulsars and is likely accurate to a factor of ~ 1.5 of the YMW16 estimate [34, 35]. Furthermore, we systematically compared pulsars with annual parallax measurements (or other more reliable distance measurements such as globular cluster association) at similar Galactic latitudes as CHIME J0630+25 to obtain the uncertainties for the YMW16 derived distances (see Methods). This results in the low dispersion measure distance of 170(80) pc. The next closest LPT is PSR J0901–4046 with a YMW16 dispersion measure distance of 330(90) pc. The uncertainties are derived with a similar method as CHIME J0630+25. CHIME J0630+25, along with PSR J0901–4046, are remarkably close and are prime candidates for multiwavelength follow-up. The existence of these two sources suggests a large Galactic population yet to be discovered.

Periodicity and timing solution

We present the phase-connected timing solution in Table 2. Despite an 802-day timing baseline, due to the large uncertainties on the arrival times of each burst and the sparse sampling, we could not robustly constrain the declination of CHIME J0630+25 through timing alone. We note that fitting a timing jump (JUMP1) to account for the clock offset for the CHIME/FRB and CHIME/Pulsar systems resulted in a value consistent with 0. This is expected as the two systems have an offset of a few hundred milliseconds, less than the arrival time uncertainty of the bursts. Therefore, we used a fixed static jump of 0.247 s, derived from timing other pulsars. The clock differences between the two systems are given a full discussion in the Methods. We also note that an additional jump at MJD 59158 can be added to reduce the residuals by a factor of ~ 2 . However, we find no physical motivation to do so as the global fit is already a small fraction of the pulse period ($< 1.5\%$).

Almost all theories for radio pulses from pulsars require the production of electron-positron pairs near the neutron star’s polar caps [5, 6, 36]. Within the context of these theories, the minimum magnetic field strengths and configurations govern the ability to generate the electron-positron pairs given a rotation period [5]. The different field configurations give rise to sets of permitted P- \dot{P} values. Possible configurations can

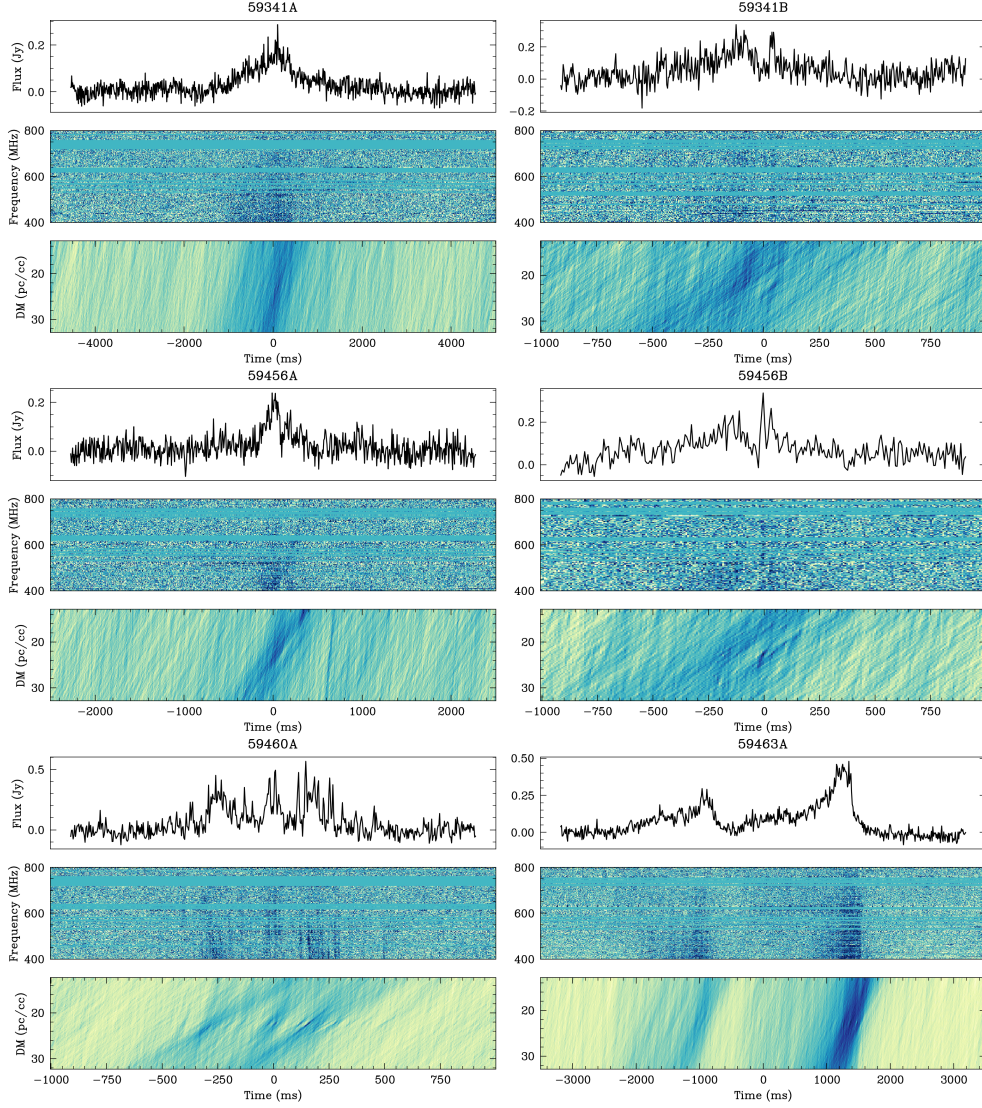


Fig. 1: The collection of pulses from CHIME J0630+25 detected by CHIME/Pulsar. The top panel for each burst contains frequency averaged and dedispersed time series. The second panel shows the dynamic spectrum of each burst, and the bottom panel show the dedispersion heat map for each burst. The dedispersion heat map shows the power for many different DM trials. All astrophysical pulses of CHIME J0630+25 pulses centre on $DM \approx 22.5 \text{ pc cm}^{-3}$.

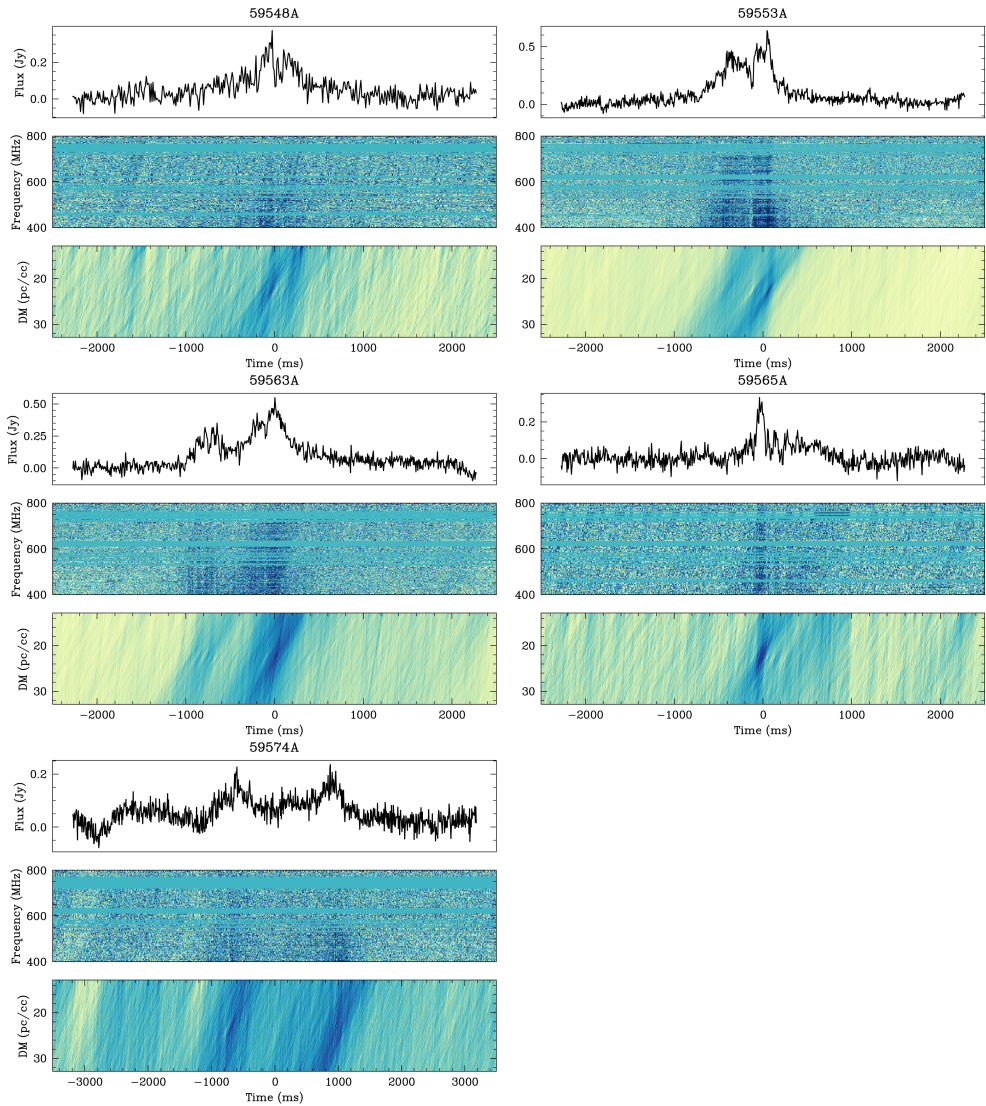


Fig. 1: continued

include dipolar, multipolar, or even twisted magnetic fields. They are complicated further as the field configuration is likely different for every pulsar due to their formation or evolution. Conventional pulsar radio emission should cease beyond some “death valley” of P - \dot{P} combination where pair production is no longer efficient [5, 6]. In Figure 2, we show the Death Valley shaded in grey for the extremes of these magnetic field configurations.

To place a conservative \dot{P} upper limit on CHIME J0630+25, we take the shifted upper limit approach as described in [37] given by $\dot{P}_{\text{upper}} = \text{MAX}(\dot{P}_{\mu}, 0) + \sigma$ where σ

Table 2: The phase-coherent timing parameters for CHIME J0630+25. The uncertainties quoted are the $1\text{-}\sigma$ confidence intervals. PEPOCH is the epoch for period determination. TIMEEPH is the time ephemeris that is used. NTOA is the number of times of arrivals used in the fit. CLOCK is the timescale that is used. JUMP1 gives the jump between the CHIME/FRB and CHIME/Pulsar instruments and is mainly determined by the single concurrent detection with both instruments. EFAC is a multiplicative factor in the TOA uncertainties. We also provide the derived parameters of τ , the characteristic age, B_{surface} , the surface magnetic field, and \dot{E} , the spin-down luminosity. However, these are strictly limits based on the shifted upper limit on \dot{P} as described in the text. The uncertainties given are those obtained from the timing fit. We did not fit the declination (see text).

Property	Value
Name	CHIME J0630+25
R.A. (hh:mm:ss)	06h30m43s±6'
Dec (dd:mm:ss)	25°23'14"
P (s)	421.35542(1)
\dot{P} ($\times 10^{-12}$ ss $^{-1}$)	-2.5(1.6)
PEPOCH(MJD)	59173
TIMEEPH	FB90
NTOA	17
CLOCK	TT(TAI)
JUMP1(s)	0.247
EFAC	2.476
reduced χ^2	1.0
Derived Values	
Galactic Longitude (deg)	188.0
Galactic Latitude (deg)	7.1
τ ($\times 10^6$ yr)	>4.2
B_{surface} ($\times 10^{15}$ G)	<0.8
\dot{E} ($\times 10^{26}$ erg/s)	<8.5

is the uncertainty given in Table 2. This results in $\dot{P}_{\text{upper}} = 1.6 \times 10^{-12} \text{ss}^{-1}$. Such a shifted upper limit regime is resilient to statistical fluctuations if one believes that the true value is near 0. As all \dot{P} measurements of other LPTs have either been positive or consistent with zero, we consider this a prudent upper limit on the \dot{P} of CHIME J0630+25. The shifted upper limit constrains CHIME J0630+25's magnetic field to be $< 0.8 \times 10^{15}$ G. Assuming that the emission is powered by spin-down, the position of

Table 3: The four X-ray sources within the CHIME J0630+25 localisation region were detected by the *Swift* XRT. see Methods for the estimated N_{H} . The maximum Galactic line of sight N_{H} is $\sim 3 \times 10^{21} \text{ cm}^{-2}$.

Source	RA hms(J2000)	Dec dms(J2000)	S/N	0.1-1.5 keV counts/s (10^{-4})	1.5-10 keV counts/s (10^{-4})	N_{H} cm^{-2}
1	06:30:49±6.8"	25:23:01±6.8"	2.8	2.4(1.9)	5.7(2.7)	$\sim 8 \times 10^{21}$
2	06:30:23±6.3"	25:25:24±6.3"	2.8	6.4(3.2)	0(2)	$< 2 \times 10^{20}$
3	06:30:28±5"	25:17:01±5"	3.2	12(4)	0.3(8)	$< 2 \times 10^{20}$
4	06:30:17±5.3"	25:19:50±5.3"	2.7	6.6(2.4)	0.0(2)	$< 2 \times 10^{20}$

CHIME J0630+25 in Figure 2 shows that it is only allowable by the twisted multiple configuration.

Magnetic white dwarfs may emit coherent radio pulses with similar mechanisms as radio pulsars [38]. Due to their larger moment of inertia, for the same spin-down, white dwarf pulsars have much more spin-down energy to draw upon for their emission. For a white dwarf, assuming that the emission mechanisms are similar to that of radio pulsars, the shifted upper limit on \dot{P} of CHIME J0630+25 would yield an upper limit on the magnetic dipole field of $\sim 3.4 \times 10^9$ G by following equation 1 in [39]. The magnetic dipole death line for a white dwarf of ~ 421 s is $\sim 3.3 \times 10^9$ G [38]. Other field configurations, such as multipole and twisted magnetic fields lower this death line. Therefore, assuming the detected emission is similar to that in regular radio pulsars, white dwarf models are much more favourable for death valley limits of CHIME J0630+25.

Quasiperiodicity

Quasiperiodicity is a feature where substructures within a burst are separated by almost an integer number of a quasiperiod. It is a common feature in radio transient phenomena on the timescales of milliseconds to seconds [16, 40, 41]. It has been suggested that quasiperiodicity may be a universal feature in neutron stars that span across multiple subclasses such as pulsars, magnetars, Rotating Radio Transients, or LPTs [41]. Some bursts of J0630+25 contain large amounts of substructure, such as 59460A. For this reason, we performed an autocorrelation analysis to search for quasiperiodicity in all bursts that show more than one peak in the burst time series (see Methods). We found no significant indications of quasiperiodicity in the 7 bursts with multiple peaks.

Swift X-ray observations

Neutron stars often emit thermal and non-thermal X-rays. Thermal emission is produced by a neutron star’s cooling surface or by hotspots such as the polar caps on the neutron star. These spots are reheated by magnetospheric return currents of accelerated charges [10]. The particles accelerated by the magnetic fields can also generate non-thermal X-ray emission independently in the form of synchrotron and curvature radiation [42–44]. Another form of non-thermal X-ray emission comes from young, energetic pulsars via the interactions between the pulsar wind and the surrounding

interstellar medium. The interactions can produce shocks that accelerate pulsar wind particles, which in turn produce X-rays [45]. All these mechanisms contribute to a vast array of neutron star high-energy emission phenomenology.

A particularly interesting subset of X-ray bright neutron stars are X-ray Dim Isolated Neutron Stars (XDINS) [46, 47]. These neutron stars are particularly close, between 100 and 500 pc away. Due to their proximity, XDINS provided precious insights into the formation pathways and thermal properties of neutron stars [48].

Driven by a similar proximity motivation as XDINS, on the 5th of November 2023, we began a 32 ks observation campaign of CHIME J0630+25 with the *Neils Gehrels Swift Observatory* X-ray Telescope (*Swift* XRT). This led to full coverage of the $1\text{-}\sigma$ localisation area of CHIME J0630+25 and partial coverage of the $2\text{-}\sigma$ localisation area. In total, we detected four X-ray sources within the $1\text{-}\sigma$ localisation area. The sources are shown in Figure 3 and Table 3. We note that source 3 is coincident with a known variable star, ATO J097.6166+25.2833. The fastest rotating stars like α Regulus and Vega possess spin periods of $\mathcal{O}(10\text{ h})$ [49, 50]. Significantly faster rotation will cause the star to lose its outer layers as it lacks sufficient centripetal acceleration [51]. Therefore, CHIME J0630+25 is unlikely to be associated with ATO J097.6166+25.2833.

As the source counts are too low to build a spectrum, we measured the counts in two different energy bands, 0.1-1.5 keV and 1.5-10 keV. We find that the majority of photons emitted by sources 2, 3, and 4 are in the lower energy bands. To compare the N_{H} of the *Swift* candidates with the DM of CHIME J0630+25, we assumed a neutron star blackbody spectrum with a temperature of 0.5 keV. This choice of blackbody spectrum was based on the data reported in the McGill Online Magnetar Catalog ⁴. We then estimated the neutral hydrogen along the line of sight using WebPIMMS ⁵ (see Methods) and found that sources 2, 3 and 4 possess low N_{H} values while source 1 is likely extragalactic. As it is likely that source 3 is associated with ATO J097.6166+25.2833, we argue that sources 2 and 4 are likely nearby and could be the X-ray counterparts of CHIME J0630+25. Deeper X-ray campaigns are required to characterise their spectra robustly.

Discussion

Timing model

From the upper limit on \dot{P} , we derived the maximum spin-down luminosity available to CHIME J0630+25 and subsequently compared this with the observed radio luminosity for both the neutron star and white dwarf models.

In the neutron star model, we derived the upper limit on the spin-down luminosity to be $8.5 \times 10^{26} \text{ erg s}^{-1}$. Using an approximate mean flux density of 0.6 mJy ⁶, the radio luminosity is estimated to be $2.2_{-1.6}^{+2.5} \times 10^{26} \text{ erg s}^{-1}$, within the spin-down luminosity range. We note, that the radio efficiency is higher than any known radio pulsar.

The emission mechanisms could also be powered by the magnetic fields of a neutron star such as the case in a magnetar. This is because the emission of CHIME J0630+25

⁴<https://www.physics.mcgill.ca/pulsar/magnetar/main.html>

⁵<https://heasarc.gsfc.nasa.gov/cgi-bin/Tools/w3pimms/w3pimms.pl>

⁶This is the flux density averaged across the period.

is highly sporadic. One such explanation is the reconnection of magnetic field lines in a neutron star’s magnetosphere, invoked to explain the emission of fast radio bursts [52]. Emission produced by drawing energy from the neutron star’s magnetic field occurs when some mechanism (e.g. magnetohydrodynamics waves) causes the reconnection of magnetic field lines in magnetospheric plasma. Once reconnection occurs, the magnetic field energy is converted into plasma kinetic and thermal energy, accelerating charged particles and releasing radiation. This could be through mechanisms such as curvature radiation [53]. Magnetars are known to emit sporadic radio emissions, for example PSR J1622–4950 [54], XTE J1810–197 [16], and SGR 1935+2154 [55]. Therefore, if the origin of the radio emission for CHIME J0630+25 is similar, it could explain the highly intermittent pulses of CHIME J0630+25. Longer timing baselines and more detections will significantly improve the \dot{P} constraint to determine a robust dipole magnetic field.

White dwarfs possess a moment of inertia roughly 1×10^5 – 5×10^5 times larger than a neutron star (assuming a range of 3000–7000 km radius for a white dwarf and 10 km radius for a neutron star). The spin-down luminosity is 0.9 – 4.3×10^{32} erg s $^{-1}$, significantly higher than the emitted radio luminosity of CHIME J0630+25. Therefore, there is more than sufficient energy in the white dwarf spin-down model.

The nature of CHIME J0630+25

Table 4: All sources that are similar in nature to CHIME J0630+25.

Source	Width FWHM (s)	P s	\dot{P} s s $^{-1}$	b °	Duty Cycle	Micro- structure	Binary	ref
ASKAP J1935+2148	10-50	3225	$< 1.2 \times 10^{-10}$	0.74	0.3–1.5%	✓	N/A	[3]
GPM 1839–10	30–300	1318	$< 3.6 \times 10^{-13}$	-2.06°	2.2–22.7%	✓	N/A	[2]
GLEAM-X ¹	30-60	1091	$< 10^{-9}$	-2.6°	2–5%	✓	N/A	[1]
CHIME J0630+25	0.2-3.2	421	$< 9 \times 10^{-13}$	$+7^\circ$	0.4–0.8%	✓	N/A	
J1912–4410	< 4	318	–	-22.06	$< 1.2\%$	–	✓	[23]
AR Scorpii	~ 60	117	3.9×10^{-13}	18.7	$\sim 50\%$	–	✓	[22]
PSR J0901–4046	~ 0.3	76	$\sim 2.21 \times 10^{-13}$	$+3.7^\circ$	$\sim 0.70\%$	✓	×	[4]
PSR J0250+5854	~ 0.070	23.5	2.72×10^{-14}	-0.5°	0.3–0.4%	–	×	[17]

¹ Abbreviation for GLEAM-X J162759.5–523504.3.

Clearly, the new population of LPTs is unexpected among the decades of pulsar, magnetar and white dwarf discoveries. Comparing CHIME J0630+25 to sources that occupy the same parameter space can offer insight into the emission source [38, 56, 57]. We provide a collection of sources which produce similar emission mechanisms in Table 4 for easy comparison. In the following section, we discuss the possibility of CHIME J0630+25 being the same class of object as actively fusing stars, Galactic Center Radio Transients, white dwarfs and neutron stars.

Many objects exhibit periodic radio emission at $\mathcal{O}(1 \text{ h})$ timescales. These include flaring ultra-cool dwarfs, like TLV 513-46546 (1.96 h), main sequence stars like CU Virginis (12.5 h) [58], and sources of unknown origin like the Galactic Centre Radio

Transients, GCRT J1745–3009 (1.3h) [59] and GCRT J1742–3001 (no period) [60]. For ultra-cool dwarfs, it has been suggested that the limit to their spin periods cannot be much less than ~ 1 h due to rotational break-up [61]. A similar argument can be given for main sequence stars at about a ~ 10 h rotational period. GCRTs are pulsing radio sources towards the Milky Way Centre. Like LPTs, their nature remains mysterious. The pulse widths of GCRT J1745–3009 are ~ 11 minutes wide and much longer than CHIME J0630+25 or any LPT [59]. Similarly, GCRT J1742–3001’s flares have widths on timescales of months, again much longer than any LPT [60]. Therefore, we conclude that none of the known source types with hour long periods can explain the properties of CHIME J0630+25.

A white dwarf origin is attractive as their rotation periods are more aligned to that of LPTs, and in particular, CHIME J0630+25 [22, 23]. AR Scorpii and J1912–4410 are the only two known radio-pulsating white dwarfs, and their rotation periods (117 s and 318 s, respectively) are within a few factors of CHIME J0630+25 [22, 23]. While AR Scorpii shows a high-duty cycle at all observed frequencies, J1912–4410 shows similar duty cycles to radio pulsars at 1.4 GHz and a high-duty cycle at higher frequencies. Therefore, at least some white dwarfs can produce radiation akin to that of radio pulsars at similar observational frequencies. We show this in Table 4. However, pulsating white dwarfs emit pulses of $\mathcal{O}(220 \text{ Jy pc}^2/\text{beam})$, more than an order of magnitude less luminous than CHIME J0630+25 [22, 23]. Note that this is only a sample of 2, and the deviations in the population of pulsating white dwarfs remain to be seen.

Both AR Scorpii and J1912–4410 are in tight binary systems, and their radio emission is thought to be an interaction between the spin frequency and the orbital frequency [23, 39]. In the case of CHIME J0630+25, we can not rule out a binary system. Indeed, if we assume circular orbits and that the timing residuals are caused by orbital motion, then an estimate of the projected semimajor axis is possible. Assuming a maximum timing residual of ~ 5 s and that Roemer delay is the main contributor to the timing residuals, we estimate that if CHIME J0630+25 were to exist in a binary, the maximum semi-major axis is ~ 0.01 AU (using equation 8.28 in [62]). This is a factor of 2 larger than the semimajor axis of AR Scorpii and J1912–4410 both at ~ 0.0055 AU. Therefore, more timing data and deeper optical surveys are required to investigate the binary white dwarf scenario for CHIME J0630+25.

We performed a cross-check with known white dwarfs compiled from Gaia EDR3 data [63] and found one viable candidate, WDJ063117.11+252250.59, within the CHIME J0630+25 localisation region. WDJ063117.11+252250.59 is located at RA=06:31:17.09 \pm 0.0004”, Dec=25:22:50.12 \pm 0.0007” with a parallax distance of 272(56) pc. The position of WDJ063117.11+252250.59 is within 2σ of CHIME J0630+25. However, despite being within 2σ of the localisation region of CHIME J0630+25, if a source is $\sim 0.5^\circ$ or more deviated from the pointing of CHIME/Pulsar beam, then we should see significant beam attenuation effects at the higher observing frequencies of CHIME/Pulsar. There are no evidence of beam effects in any of the bursts detected by CHIME/Pulsar (Figure 1), and therefore, we conclude that CHIME J0630+25 is unlikely to be associated with WDJ063117.11+252250.59. Assuming the bursts are evenly distributed in time, CHIME J0630+25 has a burst rate of ~ 0.06

bursts/h. Thus, with ~ 17 hours one can expect to make a detection at CHIME’s sensitivity. With better localisation by utilising the CHIME/FRB baseband system [64] or other interferometric telescopes, we will be able to examine the white dwarf model more conclusively.

Neutron star models for LPTs often invoke an old magnetar. Magnetars are theorised to be the early stage of neutron star evolution, and their strong magnetic fields are predicted to decay on a timescale of $\sim 10^4$ years. From spin-down alone, the maximum period of a magnetar can only reach ~ 13 s in this scenario [65]. Therefore, it has been theorised that magnetars can only reach longer periods via another mechanism, such as angular momentum kicks via giant flares [66]. Indeed, CHIME J0630+25 possess a characteristic age $> 10^6$ yr, which disfavours the magnetar model. To support the theoretical ultra long period magnetar, there is one candidate magnetar with a period of 6.67 h, 1E161348-5055 [20]. However, no radio pulsations have been seen to date. This is unsurprising as only a subset of known magnetars are radio emitters [10]. The upper limit for the surface magnetic field of CHIME J0630+25 is 0.8×10^{15} G, which allows for a magnetar-like field.

CHIME J0630+25 exhibits many similar characteristics to known Galactic magnetars and radio pulsars. Firstly, the duty cycle of CHIME J0630+25 is $\sim 0.4\text{--}0.8\%$, which is similar to known long-period pulsars such as PSR J0250+5854 and magnetar candidate PSR J0901–4046 at $0.3\text{--}0.4\%$ and $\sim 0.7\%$ respectively [4, 17]. The burst morphology of J0630+25, characterised by complex temporal and spectral structure (such as that seen in 59460A), has been documented in radio-loud magnetars such as XTE J1810–97 [16], and also the Galactic centre magnetar PSR J1745–2900 [67]. To the best of our knowledge, they have not been seen in single pulses of radio pulsars or white dwarfs.

There are some characteristics of CHIME J0630+25 which favour a regular radio pulsar rather than a magnetar. The spectral index of most bursts from CHIME J0630+25 is steep, with an average of -2.0 . Radio magnetars emit spectra which are flat even over a wide range of frequencies, from $1.4\text{--}45$ GHz [68–71]. However, most radio pulsars have steep spectra, with a mean spectral index of ~ -1.8 [72]. If CHIME J0630+25 is a neutron star, then multiwavelength observations of the source region – including spectroscopy of the *Swift*-identified X-ray sources discussed above – are essential for discerning the nature of CHIME J0630+25.

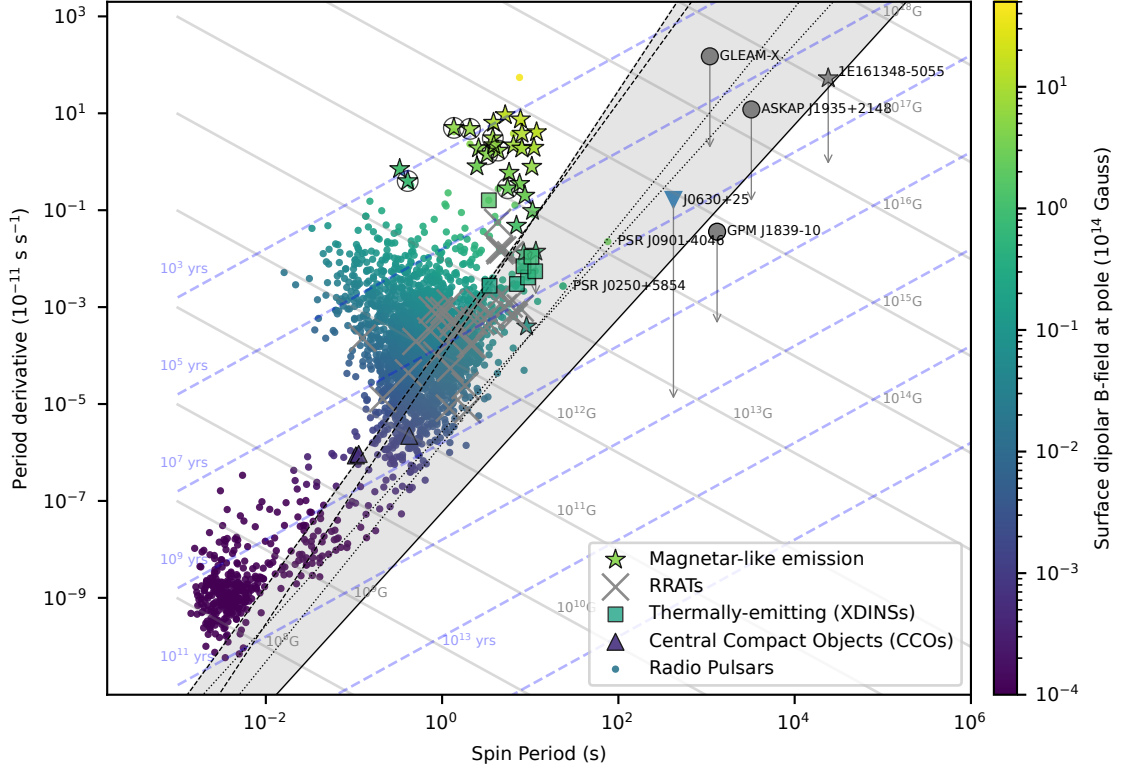


Fig. 2: The $P - \dot{P}$ diagram. 1E161348–5055, a central compact object that shows evidence of magnetar-like emission, is shown with a grey star [20]. The grey circles show the LPTs discovered by the MWA. The longest period pulsar PSR J2050+5854 and LPT PSR J0901–4046 are shown by the coloured dots and labelled as such. The grey-shaded region shows the death valley for coherent pulsed radio emission. The black dashed line corresponds to a pure dipole, dotted lines for a twisted dipole and solid lines for a twisted multipole configuration [5, 6]. The blue dashed lines correspond to lines of constant age and the grey solid lines correspond to lines of constant magnetic field. The code to create this plot was adapted from [2]¹ with more source categories (i.e. millisecond pulsars and RRATs). All downward-facing arrows correspond to upper limits and are at the 1- σ level. The CHIME J0630+25 arrow is longer to represent the shifted upper limit used (see text)

¹<https://github.com/nhurleywalker/GPMTransient>

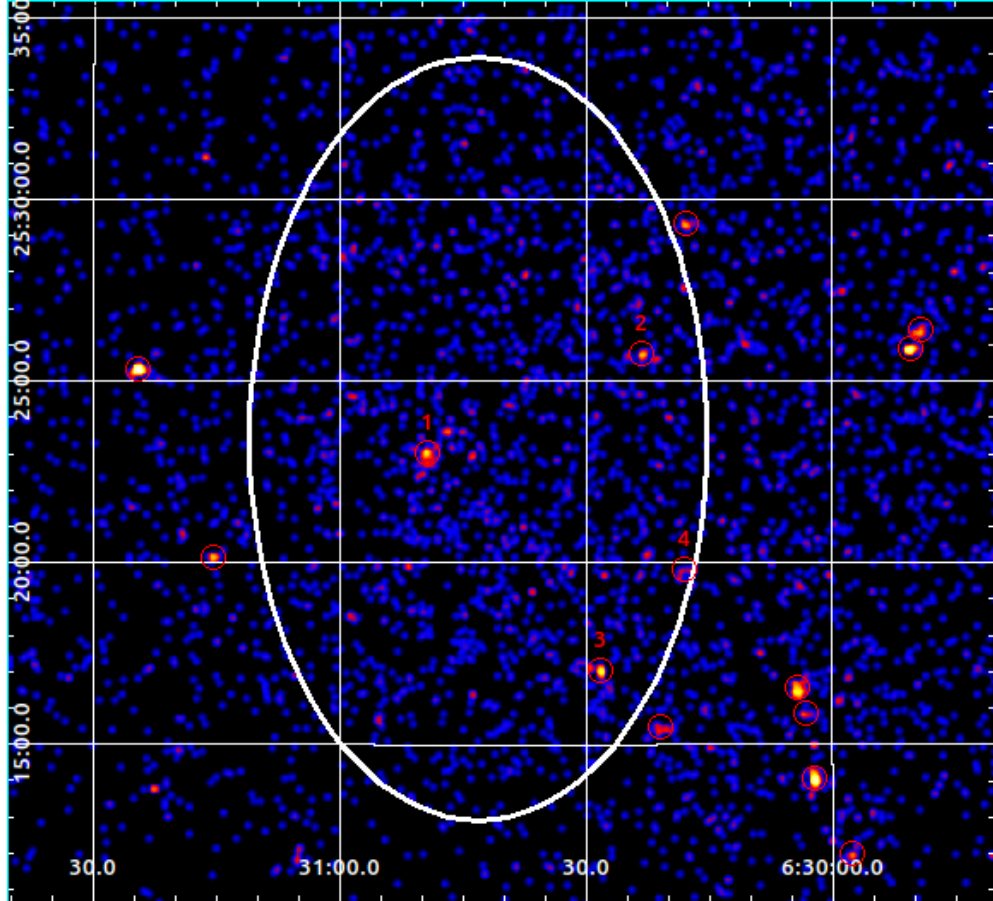


Fig. 3: The *Swift*-XRT observations with detected sources and the CHIME J0630+25 localisation region overlaid. The localisation uncertainty region for right ascension is from pulsar timing, and the declination uncertainty region is from multi-beam detections of J0630+25 with CHIME/FRB (see Methods). The sources are numbered to match those in Table 3.

Methods

Source Identification

CHIME/FRB is a trigger-based FRB-detection instrument on the CHIME telescope [25] that constantly scans the overhead sky with 1024 FFT-formed beams between 400–800 MHz and a field of view of approximately 2° in RA and 100° in Dec [26]. The instrument triggers on any impulsive signal that passes the initial radio frequency interference (RFI) check [26]. Then, bespoke software will determine if the incoming signal is terrestrial or astrophysical in nature. Data are then saved to disk if a certain S/N threshold (currently 8.5) is met. Due to the substantial data volume, data for sources within the Milky Way Galaxy were not saved by CHIME/FRB until October 2022. However, metadata were saved for each “event” regardless of origin. The metadata contains real-time pipeline-derived information such as the RA, Dec, DM, TOA, and S/N. We used the CHIME Metadata Clustering Analysis (CHIMEMCA), to identify CHIME J0630+25 [see 24, for a full description]. After filtering out RFI, a cluster was identified by CHIMEMCA, with the first event of the cluster detected on MJD 58772 at 12:54:51 UTC, at RA=06:30:19±30′ and Dec=25:23:14±30′ with a DM of (22.6 ± 3.2) pc cm⁻³.

The CHIME/Pulsar instrument forms ten steerable phased array tracking beams to track sources as they pass through the CHIME field of view. It produces high-time resolution spectra, packaged as conventional SigProc-style filterbank data⁷. CHIME/Pulsar can also correct for intrachannel dispersion smearing through coherent dedispersion and can record data at significantly higher time resolutions than CHIME/FRB. These advantages, along with the phased array tracking beams, contribute to an increase in sensitivity for CHIME/Pulsar compared to CHIME/FRB.

Follow-up observations were conducted using the CHIME/Pulsar system from MJD 59300 to MJD 60116. These observations were carried out nearly daily, consisting of about 10 minutes per scan, resulting in 688 observations and 175.946 hours of Stokes I data for this study. To process all the CHIME/Pulsar data, we have employed the CHIME/Pulsar Single-pulse PIPEline (CHIPSPIPE)⁸, an automated single-pulse search pipeline designed to handle the large data volume of CHIME/Pulsar. The pipeline is based on PRESTO [73]. It further utilises SPEGID [74] and FETCH [75] to filter out spurious candidates. Finally, the pulses that are graded as astrophysical by FETCH are examined by a human. For a detailed discussion of CHIPSPIPE, refer to [24]. For all the bursts that passed the human check, we manually removed the RFI-contaminated channels and generated the dynamic spectrum, pulse profile, and dedispersion-time plot for each burst using the Your [76] package. These are shown in Figure 1.

CHIPSPIPE has limited sensitivity to wider pulses. Therefore, we visually inspected the dynamic spectrum and pulse profile around each detected pulse within a 10-second window. This manual inspection aims to identify additional sub-pulses missed by CHIPSPIPE that may provide evidence of quasiperiodicity. 59460A,

⁷<https://sigproc.sourceforge.net/>

⁸https://github.com/CHIME-Pulsar-Timing/CHIME-Pulsar_automated_filterbank

Table 5: This table shows the results of fitting for the quasiperiodic peaks in the auto-correlation function. The X_i parameters are the location parameters for the Gaussian peak in the ACF. The σ parameters are the width parameters for the peaks in the ACF. 59460A is the only burst with two peaks in the intensity time series and, therefore, is the only burst with two X_i parameters.

Burst	X_0 ms	σ_0 ms	X_1 ms	σ_1 ms
59460A	206^{+7}_{-8}	88^{+8}_{-7}	440^{+10}_{-10}	123^{+7}_{-7}
59463A	2490^{+10}_{-10}	504^{+20}_{-10}	–	–
59553A	376^{+2}_{-2}	209^{+3}_{-2}	–	–
59563A	760^{+10}_{-10}	270^{+20}_{-20}	–	–
59574A	1460^{+60}_{-60}	410^{+100}_{-80}	–	–

59463A, 59553A, 59563A, and 59574A exhibited distinct second peaks not flagged by the initial CHIPSPIPE detection.

In total, with CHIME/FRB, we detected 6 bursts above S/N 8.5, and with CHIME/Pulsar, we detected 11 bursts with Stokes-I intensity data showing extended widths and complex structures, typical of other LPTs. Despite the lack of Stokes-I intensity data, we confirmed the CHIME/FRB bursts to be real astrophysical events as the arrival time is consistent with the rotation period of CHIME J0630+25. All bursts are detailed in Table 1. Subsequent localisation with the CHIME/FRB metadata [28] yielded RA=06:31:00±6', Dec=25:23:24±11' in J2000 coordinates at the 1σ level. Considering that the disparity between the CHIME/Pulsar pointing and the CHIME/FRB localisation is roughly equivalent to one full width at half maximum of the CHIME/Pulsar beam at 400 MHz [27], it is likely that the true location of the source lies between the localisation made by CHIME/FRB and the CHIME/Pulsar pointing. Indeed, the long-term timing of CHIME J0630+25 suggests that the best fit RA is 06:30:43±6' (see Section 21), which is taken to be the preferred RA localisation throughout this study. Interferometric telescopes with low-noise environments, such as the Karl Jansky Very Large Array or MeerKAT, should be able to localise CHIME J0630+25. Furthermore, we are currently saving CHIME/FRB baseband data, which will allow for more precise localisation of future detections.

Quasiperiodicity

This section aims to identify any quasiperiodicity in the bursts emitted by CHIME J0630+25. We began our analysis by visually examining the bursts. This initial step allowed us to identify distinct burst morphologies, which we then categorised into three groups: C1, C2, and C3. C1 represents bursts with a single clear peaked envelope. C2 bursts are double-peaked, where the second peak builds on top of the first without returning to the baseline. Finally, C3 bursts occur when the pulse rises, reaches a peak,

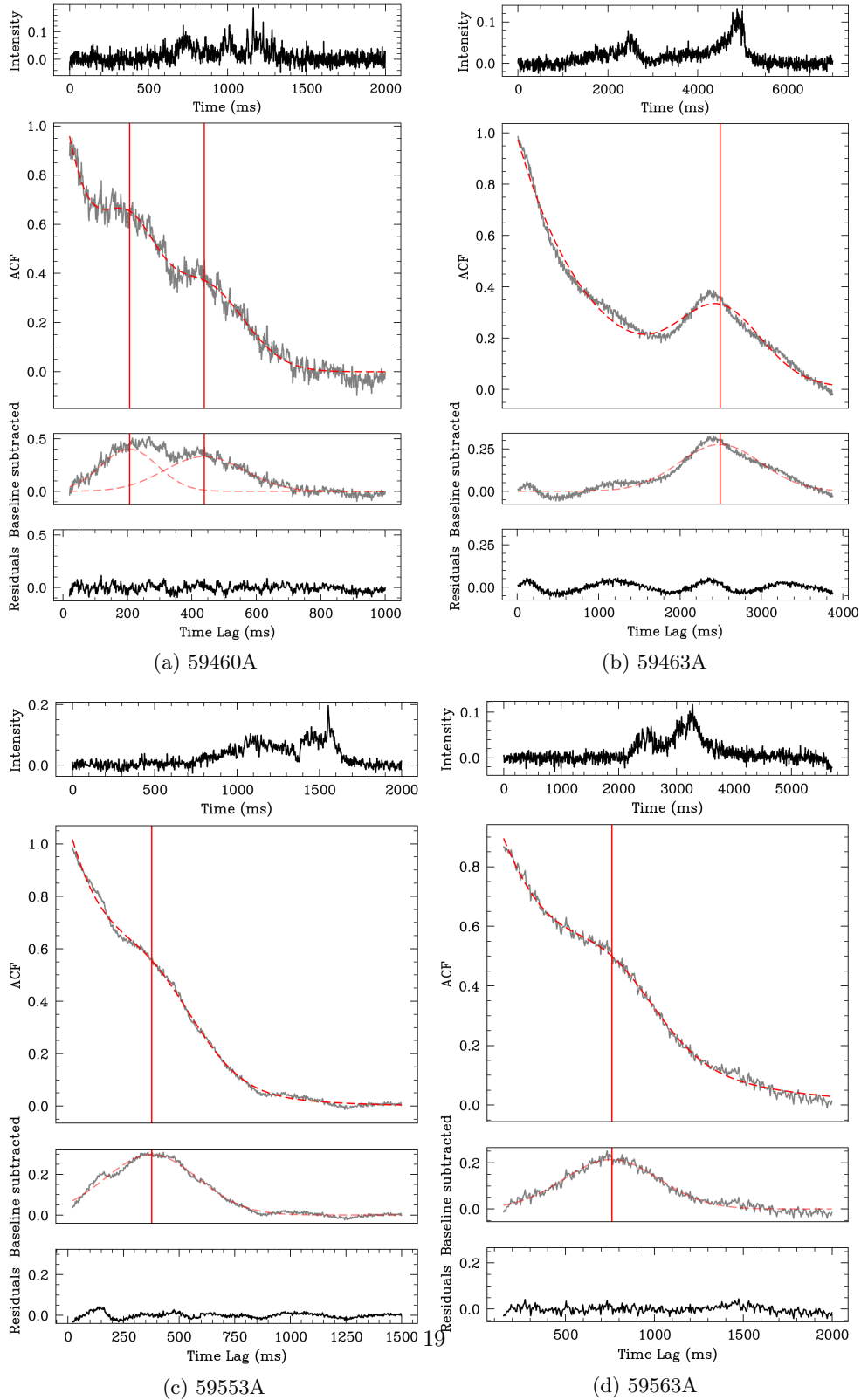
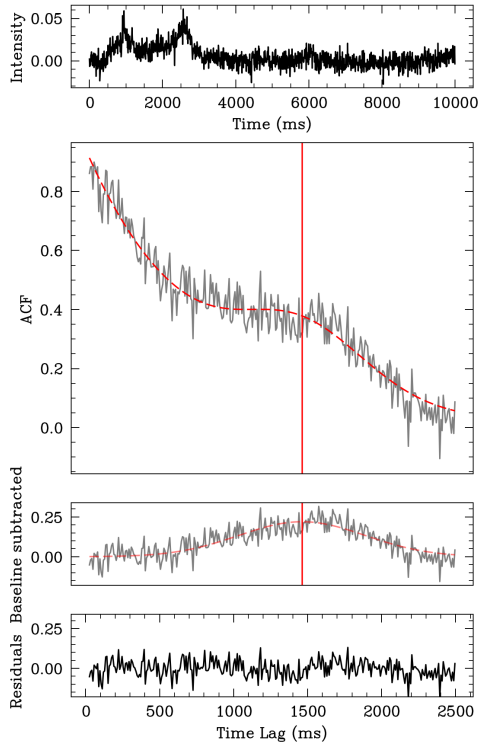


Fig. 4: Autocorrelation on the band-averaged time series of C2 and C3 type bursts. The top panel for each burst is the band averaged intensity, and the second panel is the autocorrelation, where the dashed red line is the Gaussian modulated exponential decay that has been fitted. The third panel subtracts the exponential decay from panel two, leaving only the Gaussian component. The bottom panel is the residual after all components of the fit have been subtracted. The red vertical lines represent the location of the fitted Gaussian. The residuals still exhibit a small amount of structure. This is generally an order of magnitude smaller than the subtracted signal and is the result of two factors: the variable CHIME/Pulsar baseline and not being able to exactly describe the ACF peak as a Gaussian (such as is the case for 59463A and 59553A).



(e) 59574A

Fig. 4: continued

falls back to near baseline, and exhibits a second peak (and, in the case of 59460A, a third). Among the bursts analysed, we found three (59553A, 59563A, and 59574A) exhibiting C2 behaviour and two (59460A and 59463A) exhibiting C3 behaviour and — the rest exhibit C1 type behaviour. The categories are tabulated in Table 1.

In the subsequent analysis, only the bursts belonging to the C2 and C3 categories are used. We examined the separation between the peaks in C2 and C3 bursts by performing autocorrelation on each burst. The autocorrelation results are presented in Figure 4. The second panel shows the autocorrelation function (ACF) result for each burst. To extract the separation between peaks, we fitted an exponential decay modulated by a Gaussian function to the ACF using Bayesian Markov Chain Monte Carlo (MCMC) with uniform priors. The fit model is described by

$$f(T) = A \exp(-BT) + C \exp\left(-\frac{(T - X_0)^2}{2\sigma_0^2}\right) \quad (1)$$

for all bursts apart from 59460A or

$$f(T) = A \exp(-BT) + C \exp\left(-\frac{(T - X_0)^2}{2\sigma_0^2}\right) + D \exp\left(-\frac{(T - X_1)^2}{2\sigma_1^2}\right) \quad (2)$$

in the case of 59460A. $A, B, C, D, X_0, \sigma_0, X_1, \sigma_1$ are fit parameters and T is the time-lag parameter. The X parameters give the separation between sub-bursts. The σ parameters give the width of the fitted Gaussian. 59460A requires a two Gaussian fit due to the three peaks in the intensity time series. The exponential baseline is removed for each burst and is shown in the respective third panels of Figure 4. This leaves only the Gaussian (peak) component behind. A, B, C , and D are nuisance parameters and are marginalised over to provide the fit results in Table 5.

Interestingly, we found that the peak time lag in 59563A is a factor of 2.02(4) greater than that of 59553A, and the peak time lag in 59574A is a factor of 1.9(1) greater than that of 59563A. We then tested the significance of this apparent factor of two. We simulated five different sub-burst separations between 180 ms, the narrowest burst detected, and 10,000 ms, the search range for additional sub-bursts. We then assigned a sub-burst arrival time for each sub-burst, i.e., if one of the simulated burst separations was 760 ms, the TOAs assigned would be 0 ms and 760 ms. Therefore, for five sub-burst separations, we get five pairs of TOAs. We then found every combination of three sub-burst separations pairs. There are $\binom{5}{3} = 10$ combinations. For each combination, the TOA pairs were inputted into `rrat_period_multiday`, a sub-program of PRESTO. `rrat_period_multiday` was designed to find any underlying periodicity for many sets of single-pulse arrival times and will provide the most likely period and the separation between bursts [77, 78]. When the period calculated by `rrat_period_multiday` results in all separations within 0.1 of an integer number, we counted that as a success. If there is one success within the $\binom{5}{3}$ combinations, then that trial was successful. We performed 1,000,000 trials with 982,002 successes. This indicates that the situation where there is a common integer factor between the three different burst separations is highly likely and, thus, is not significant.

Distance determination and dispersion measure

For the distance determination, the dispersion measure used is the error-weighted average of all the CHIME/Pulsar detections. This is given by

$$DM_{av} = \frac{\sum_i DM_i / \sigma_i^2}{\sum_i 1 / \sigma_i^2}. \quad (3)$$

Where DM_i is the dispersion measure of each individual pulse and σ_i is the corresponding uncertainty. The average uncertainty is given by

$$\sigma_{DM} = \frac{1}{\sqrt{\sum_i \sigma_i^2}}. \quad (4)$$

The resultant DM value is 22(1) pc cm⁻³.

The distance was determined by the YMW16 electron density model [33]. To find the uncertainties associated with CHIME J0630+25, we queried the ATNF pulsar catalogue and applied a series of cuts to the full catalogue. First, we isolated those pulsars with similar Galactic latitudes as the $b = 7^\circ$ of CHIME J0630+25. We selected pulsars with $b > 4^\circ$ and $b < 10^\circ$. We then limited the DM of these sources to be less

than 60 pc cm^{-3} . Finally, we only considered pulsars with an independent distance measure, such as parallax or globular cluster association. In total, 10 pulsars met this criteria. We then defined the uncertainty of CHIME J0630+25 as the standard deviation of CHIME J0630+25 if it were to possess the same fractional uncertainty as the 10 pulsars. Explicitly this is

$$\sigma_{\text{J0630+25}} = \sqrt{\sum_i^N \frac{\left(170 \text{ pc} \times \frac{d_i}{y_i} - \mu\right)^2}{N}} \quad (5)$$

where d_i is the independently measured distance to the pulsar, y_i is the YMW16 derived distance, μ is the mean of all $170 \text{ pc} \times \frac{d_i}{y_i}$, and N is the total number of pulsars which meet the defined criteria. For CHIME J0630+25, we found that the distance is $170(80) \text{ pc}$. Note that the 1 pc cm^{-3} uncertainty on the DM translates to a deviation of 2 pc according to the YMW16 electron density model and, therefore, is negligible compared to the uncertainty due to the electron density model itself. Therefore, is not included in the final value. Applying this error determination method to the 10 pulsars in our sample, we find that the true position of all but one source is within $2\text{-}\sigma$ of the YMW16 distance estimate.

Timing

The time of arrival (TOA) extraction is vital for period determination and timing solution extraction. This is necessary for both the CHIME/FRB and CHIME/Pulsar datasets. Unfortunately, for the CHIME/FRB detections, the only data products saved were the metadata. These contain a timestamp but no total intensity data, and therefore it is difficult to know if the system triggered on one of the microstructure peaks. The complex and long burst widths of CHIME J0630+25 mean that CHIME/FRB could have triggered on any one of the microstructure peak components within the burst envelope. Therefore, we took a conservative TOA error of 1 s for all metadata-only detections. The CHIME/FRB TOAs are referenced at the bottom of the CHIME band at 400 MHz. For the CHIME/Pulsar detections where the total intensity data are recorded, we followed the prescription outlined in [2]. Specifically, we smoothed the bursts' pulse profile using a 1-s Gaussian kernel. The maximum of the smoothed profile is taken as the TOA, and the full-width-half-max (FWHM) is taken as the uncertainty of the TOA. The CHIME/Pulsar TOAs are referenced at the top of the CHIME band at 800 MHz. In total, we collected 11 TOAs spread over 802 days between MJD 58772 and 59574. All TOAs are then corrected to the solar system barycentre arrival time using `Astropy` for use with `rrat_period`.

The next step is to generate the full timing ephemeris. Using the `rrat_period` module of `PRESTO` with the barycentre corrected TOAs of all CHIME/Pulsar bursts, we found that the most likely period for CHIME J0630+25 is $\sim 421 \text{ s}$. The derived period is only approximate as `rrat_period` provides only an estimated period without accounting for period derivatives. On two occasions, CHIME/Pulsar observed two bursts during the same transit. These are MJD 59341A, B and MJD 59456A, B,

separated by 422.5(2.2) s and 418.2(1.4) s, respectively, driving the convergence to 421 s. Taking this as a starting point, we created a timing ephemeris, with the period derivative set to 0 and one phase jump (JUMP1) between the CHIME/Pulsar and CHIME/FRB instruments. We tested the validity of fitting the phase jump between the two instruments by performing the same TOA extraction procedure described above on multiple pulsars, namely J0012+54, J0209+5759, and J1838+5051. During this process, we ensured that the timespan covered was similar to that of CHIME J0630+25. Then, using PINT, a jump is fit between the CHIME/FRB and CHIME/Pulsar TOAs of the three pulsars. The fitted jumps for all three pulsars are 0.215(2) s, 0.250(6) s, and 0.272(2) s, respectively. For the timing of CHIME J0630+25 we use a fixed 0.247 s clock offset between the CHIME/FRB and CHIME/Pulsar TOAs. This is the mean of the jumps fit for the three pulsars.

We then used two standard pulsar timing software, PINT ⁹[30] and TEMPO2 ¹⁰ [29], to perform a least squares fit to all the TOAs of J0630+25. The results for the fit are provided in Table 2, and the residuals are provided in Figure 5. We noticed a slight downward drifting trend before MJD 59168. Therefore, we tried to fit the second period derivative, however it did not provide significant improvements.

To test the significance of the 421 s period, we calculated the probability that an alternative period will always be detected as an integer multiple of 421 s. We defined the alternative period as $P2 = P_{J0630+25}/i$ where $P_{J0630+25}$ is the period given in Table 2 and i is an integer factor. We also accounted for the timing noise shown in Figure 5 by allowing the detection to be made within 6 s (roughly the worst residual of all the TOAs) of an integer multiple of 421.35542 s. If CHIME J0630+25 had a true period of 421.35542 s/ i then the probability that a pulse lands precisely on a multiple of 421.35542 is 1/ i . Because we allowed it to land anywhere within 6 s of an integer multiple of 421.35542 s the probability is therefore $(2 \times \text{int}(6/P2) + 1)/i$. Where int is the integer flooring function. The first burst does not contribute to the probability as it sets the starting point. Therefore, the probability that a source with an alternative period will always be detected within 6 s of an integer multiple of 421.35542 s is

$$P_i = \left(\frac{2 \times \text{int}(6/P2) + 1}{i} \right)^{N-1} \quad (6)$$

where N is the number of detections made. The alternative period can vary between $i=2$ to $i=210$ such that the smallest alternative period is the largest FWHM of any burst. We then account for the look-elsewhere effect by calculating the probability of any alternative period defined by

$$P_{\text{any alternative}} = 1 - \prod_{i=2}^{210} (1 - P_i). \quad (7)$$

Only using the 11 bursts from CHIME/Pulsar, the probability of any alternative period is 0.00099. This is dominated by $P_2 = 0.00097$ and rapidly decays for all other alternative periods. Therefore, we conclude that 421.35542 s is the correct period for CHIME J0630+25.

⁹<https://github.com/nanograv/PINT>

¹⁰<https://ascl.net/1210.015>

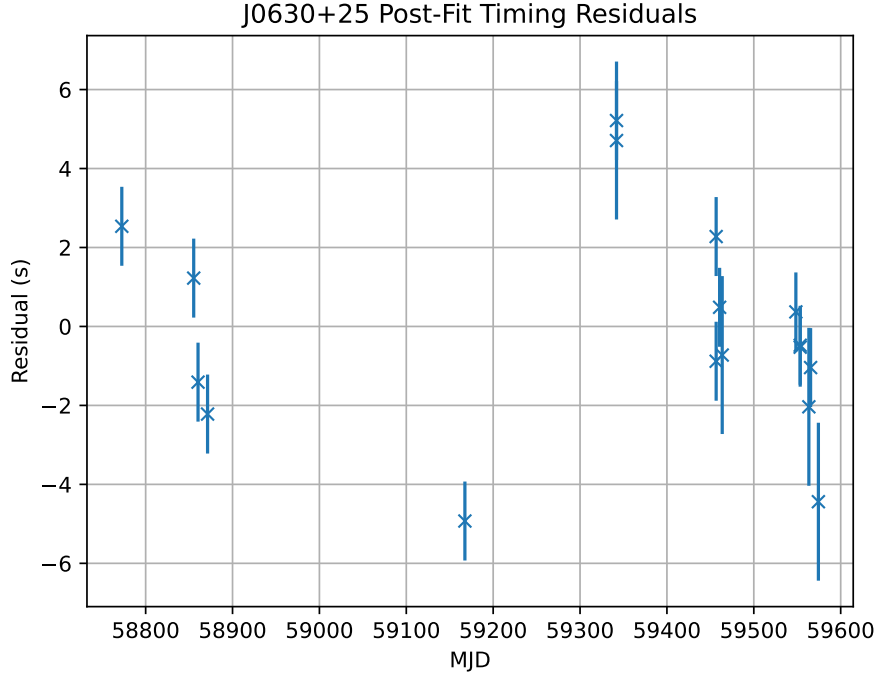


Fig. 5: The timing residuals for CHIME J0630+25. The plot shows the residuals of the phase-connected timing parameters in Table 2.

DM Measurement and Flux Calibration

Using the total intensity data obtained by CHIME/Pulsar, we measured some essential characteristics such as effective pulse width, fluence, and DM. For the bursts detected from CHIME J0630+25, the fluence is defined by the integrated flux density over the duration of the burst, and the effective width is calculated via $W_{\text{eff}} = F/S_{\text{peak}}$ where F is the fluence and S_{peak} is the peak flux density.

CHIME/Pulsar has declination-dependent sensitivity. Therefore, we used 3C133 as a calibrator source to determine the system equivalent flux density (SEFD). The SEFD is calibrated by fitting the telescope temperature and is defined in the following way

$$\text{SEFD}(\nu) = \frac{T_{\text{telescope}}(\nu) + T_{\text{sky}}(\nu)}{G(\nu)} \quad (8)$$

where T_{sky} is obtained from the Haslam 408-MHz all-sky map [79, 80], $G \approx 1.16$ K/Jy is the telescope gain and $T_{\text{telescope}}$ is the system temperature of all telescope components (i.e. receiver, structure, ground etc). The flux density of a steady source is given by

$$S(\nu) = \frac{T_{\text{on}}(\nu) - T_{\text{off}}(\nu)}{T_{\text{off}}(\nu)} \times \text{SEFD}(\nu), \quad (9)$$

where $S(\nu)$ is the flux density. T_{on} and T_{off} are the temperatures of the calibrator source and a blank patch of nearby sky, respectively. $T_{\text{telescope}}$ is an unknown, thus, we performed a maximum likelihood reduced χ^2 fit of the CHIME/Pulsar measured 3C133 spectrum against the catalogued flux density measurements of 3C133. For the catalogue values, we used the VLA calibrator list ¹¹. We found that the best functional form of $T_{\text{telescope}}$ is a 5th-order polynomial. We then used the single pulse radiometer equation to convert from S/N units to Jy units for each burst,

$$S(\nu) = \frac{S/N}{\sqrt{n_p \Delta\nu \Delta t}} \cdot \text{SEFD}(\nu) \quad (10)$$

where S/N is the signal to noise ratio, n_p is the number of polarisations, $\Delta\nu$ is the bandwidth, and Δt is the time resolution.

We measured the DM of each pulse using `DM_phase` ¹² which is a brute force algorithm that maximises the coherent power across the bandwidth by trying many different DMs. Due to the wide burst widths, the DM uncertainty for each pulse is large; this is exemplified in Figure 1 by the large hot spot that the dedispersion panel covers.

Spectral index

Using the total intensity data for the CHIME/Pulsar bursts, we measured the spectral index of CHIME J0630+25. We first flux calibrated the bursts using the method described above. This process will also serve to calibrate the spectrum of CHIME J0630+25. Then, each burst is integrated over its duration to obtain a spectrum. Maximum likelihood is used to fit the spectra with a power law model of the form

$$S(\nu) = A\nu^\alpha \quad (11)$$

where α is the spectral index, and A is the amplitude parameter. Both α and A are fit parameters. The spectral indices are provided in Table 1. All spectral index fits are provided in the Appendix.

To place an uncertainty on the fit, we measured the spectral index of 23 other calibrator sources with known spectral indices using the same technique. We found that the mean uncertainty on the spectral index calibrated in this way is 0.3.

Energy Budget

The upper limit of the spin-down energy is given by [62]

$$\dot{E} = -4\pi^2 I \dot{P} / P^3 \quad (12)$$

where I is the moment of inertia of the neutron star, P is the period, and \dot{P} is the period derivative. The moment of inertia is assumed to be $I = 10^{45}$ g cm², the period

¹¹<https://science.nrao.edu/facilities/vla/observing/callist>

¹²https://github.com/danielemichilli/DM_phase

is 421.35542 s, and the period derivative is given by the conservative shifted upper limit of $1.6 \times 10^{-12} \text{ s s}^{-1}$. This yields an upper limit on the spin-down energy of $8.5 \times 10^{26} \text{ erg s}^{-1}$.

We followed the prescription laid out in Equation 3.40 of [62] for the estimated radio luminosity. This is given by

$$L = \frac{2\pi d^2}{\delta} (1 - \cos\rho) S_{\text{mean}}(f_0) \frac{f_0^{-\zeta}}{\zeta + 1} (f_2^{\zeta+1} - f_1^{\zeta+1}), \quad (13)$$

where L is the total radio energy output, d is the distance, ρ is the opening angle, δ is the duty cycle, f_0 is 600 MHz for CHIME, S_{mean} is the mean flux density at f_0 , $\zeta = -2$ is the mean spectral index, and $f_1 \approx 10^7 \text{ Hz}$ and $f_2 \approx 10^{11} \text{ Hz}$ are reference frequencies. For the duty cycle, we took the largest FWHM of the collection of CHIME J0630+25 pulses, i.e., $\delta = W/P \approx 4 \text{ s}/421 \text{ s} = 9.5 \times 10^{-3}$. Assuming typical opening angles of $\rho \approx 6^\circ$ [62], an observing frequency of 600MHz, mean flux density of 0.0006 Jy (calculated by the average fluence/period), and a distance of 0.17 kpc, we found

$$L \approx 1.2 \times 10^{31} \text{ erg s}^{-1} (0.17 \pm 0.08 \text{ kpc/kpc})^2 (0.0006 \text{ Jy/Jy}) = 2.2_{-1.6}^{+2.5} \times 10^{26} \text{ erg s}^{-1} \quad (14)$$

Therefore, the total radio luminosity output of CHIME J0630+25 is within the spin-down luminosity range.

Follow up of CHIME J0630+25 with other telescopes

We use data from both archival observations near CHIME J0630+25 and targeted follow-up campaigns to explore CHIME J0630+25 across many wavelengths. In the radio band, we used the Green Bank Telescope (GBT) because of its increased sensitivity and longer observation tracks compared to CHIME. We also used the upgraded Giant Metrewave Radio Telescope (uGMRT) and archival VLA Low-band Ionosphere and Transient Experiment (VLITE) to localise CHIME J0630+25. Both uGMRT and VLITE can reach arcsecond angular resolution.

Pulsars and magnetars are known to emit X-rays. Therefore, we also performed targetted observations with the Neils Gehrels Swift Observatory's X-Ray Telescope (XRT). Finally, some magnetars are soft γ -ray repeaters. Thus, we searched the known γ -ray archives for as-of-yet-unknown magnetar candidates.

Radio

We were awarded 16 hours of observations using the GBT at 800 MHz and 16 hours at 1440 MHz to observe CHIME J0630+25. We used the VEGAS back end at 20.48 μs time resolution and coherently dedispersed to 22.5 pc cm^{-3} . The observations were taken between MJD 59861 and 59914. The Stokes I data were processed using CHIPSPIPE to search for single pulses. No pulses were detected.

We were also awarded 12 hours of data with the upgraded Giant Metrewave Radio Telescope to localise the source. We performed the observations between MJD 59700 and 59837 from 950 MHz to 1460 MHz. These had an integration time of 0.67 s in incoherent array mode. Unfortunately, due to the variable baseline and the high levels

Table 6: Properties of all telescopes used for this study

	CHIME/FRB	CHIME/Pulsar	GBT L-band	GBT 800MHz	VLITE 338 MHz
Receiver noise temperature	~50K	~50K	~18K	~20K	~180K
Frequency Range	400-800MHz	400-800MHz	1150-1730MHz	680-920MHz	321.9-360MHz
Number of beams	1024 (Static)	10 (Tracking)	1	1	1
Beam width (FWHM)	40'-20'	30'-15'	9'	15'	5''
Time resolution	1ms	327.68 μ s	20.48 μ s	20.48 μ s	2s
Search Frequency Resolution	24.4 kHz	390.625 kHz	781 MHz	195 MHz	47.1 MHz
Coherent Dedispersion	No	Yes	Yes	Yes	No

of radio frequency interference (RFI), we were not able to make use of the uGMRT data.

Finally, we searched through archival data from VLITE [81, 82]¹³ for high-resolution observations ($\sim 5''$) at 340 MHz covering the region of interest. We identified two observations where CHIME J0630+25 was located within 2° of the phase centre and made short time interval images at the VLITE sample time of 2 s. The short VLITE images were catalogued using PyBDSF [83], and components associated with all persistent radio sources were eliminated. The remaining catalogued sources were low signal-to-noise ($S/N \sim 4$), and visual inspection revealed these remaining candidates were likely associated with poorly cleaned sidelobes in the images. As the CHIME/FRB localisation is large compared to the VLITE resolution, the chance coincidence for a low S/N candidate is large. Therefore, it is difficult to associate any low S/N VLITE candidates with CHIME J0630+25. Unfortunately, VLITE's highest time resolution is 2 s and so bursts from CHIME J0630+25 are predominantly less than one bin long, resulting in low S/N . This makes it challenging to differentiate potential CHIME J0630+25 bursts in VLITE data from remaining uncleaned sidelobe structures.

X-ray

Our X-ray observations of CHIME J0630+25 consisted of 32ks of Swift XRT time under target ID 97140 and 97203. The two targeted observations allowed comprehensive RA coverage over the large uncertainty area of CHIME J0630+25. To process the data, we used the tools provided by the UK Swift Science Data Centre¹⁴ to create the images. Then, we used `Ximage`¹⁵ to detect the sources and provide S/N estimates. The final image (Figure 3) was produced using `Saoimage DS9`¹⁶.

To measure the count rates at 0.1-1.5keV and 1.5-10keV, we created the images using the UK Swift Science Data Centre image creation package. Then, using `Ximage` and the `sosta` program, we estimated the localised count rate and background in the local region of the sources. We then used the `WebPIMMS`¹⁷ software to estimate the neutral hydrogen along the line of sight for each of the sources. This was done by

¹³<https://vlite.nrao.edu>

¹⁴https://www.swift.ac.uk/user_objects/

¹⁵<https://heasarc.gsfc.nasa.gov/docs/software.html>

¹⁶<https://sites.google.com/cfa.harvard.edu/saoimageds9>

¹⁷<https://heasarc.gsfc.nasa.gov/cgi-bin/Tools/w3pimms/w3pimms.pl>

assuming a black body spectrum of 0.5 keV. Then, we entered an input energy range of 0.1-1.5keV and an output energy range of 1.5-10keV. We then adjusted the Galactic N_{H} value until we found a reasonable match with the observed hardness ratio.

γ -ray

We also searched for possible as-of-yet unknown soft γ -ray repeater counterparts to CHIME J0630+25. These would reside in the same databases as γ -ray bursts (GRB), albeit with an unknown classification. We first cross-match the coordinates and times of arrivals of CHIME J0630+25 with all γ -ray sources reported in GRBWeb [84]. We limit the GRBWeb triggers to those that are well localised (e.g., 1σ spatial error < 1 degree), as it is challenging to claim significant spatial coincidences for triggers with either unknown or large uncertainty regions. In our cross-match, we conservatively assume a 1σ positional error in RA of 1 degree and a 1σ positional error in DEC of 0.5 degrees for CHIME J0630+25. We then cross-match the localisation region of CHIME J0630+25 with that of all known sources in GRBWeb, requiring the localisations to be consistent within the 3σ uncertainties. Within one week of each burst, we did not find any sources to be coincident with CHIME J0630+25. However, given GRBWeb's focus on cosmological GRBs and not Galactic γ -ray sources such as soft γ repeaters, we also cross-match the position of CHIME J0630+25 and its bursts with all triggers reported in the γ -ray Coordination Network (GCN)¹⁸ circulars. We again limit our search to well-localised triggers, e.g., ($\sigma < 1$ degree), and do not find any trigger-burst pairs with the given criteria. When considering solely spatial coincidence, however, we find one trigger spatially coincident with CHIME J0630+25. The trigger is GRB110414A, which was detected long before CHIME was built.

However, as noted in [85], there is a high chance probability of finding spatial coincidences given CHIME's current localisation capabilities. Accordingly, we conclude that no significant coincidences exist between CHIME J0630+25 and any known γ -ray triggers.

Acknowledgements

F.A.D is support by the UBC Four Year Fellowship.

Basic research in radio astronomy at the U.S. Naval Research Laboratory is supported by 6.1 Base funding. Construction and installation of VLITE was supported by the NRL Sustainment Restoration and Maintenance fund.

Pulsar and FRB research at UBC are supported by an NSERC Discovery Grant and by the Canadian Institute for Advanced Research.

K.S. is supported by the NSF Graduate Research Fellowship Program.

A.B.P. is a Banting Fellow, a McGill Space Institute (MSI) Fellow, and a Fonds de Recherche du Quebec – Nature et Technologies (FRQNT) postdoctoral fellow.

V.M.K. holds the Lorne Trottier Chair in Astrophysics & Cosmology, a Distinguished James McGill Professorship, and receives support from an NSERC Discovery grant (RGPIN 228738-13), from an R. Howard Webster Foundation Fellowship from CIFAR, and from the FRQNT CRAQ.

¹⁸www.gcn.gsfc.nasa.gov

The Dunlap Institute is funded through an endowment established by the David Dunlap family and the University of Toronto. B.M.G. acknowledges the support of the Natural Sciences and Engineering Research Council of Canada (NSERC) through grant RGPIN-2022-03163, and of the Canada Research Chairs program.

A.M.C. is funded by an NSERC Doctoral Postgraduate Scholarship.

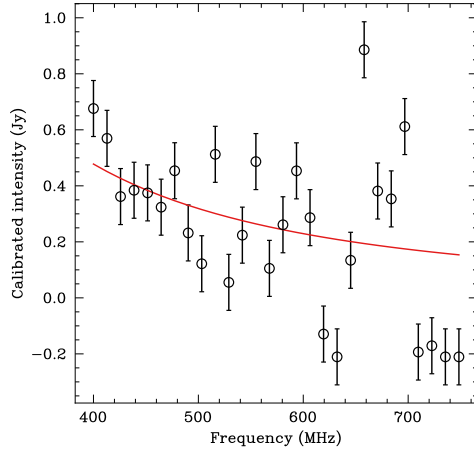
S.M.R. is a CIFAR Fellow, and is supported by the NSF Physics Frontiers Center award 2020265.

K.W.M. holds the Adam J. Burgasser Chair in Astrophysics.

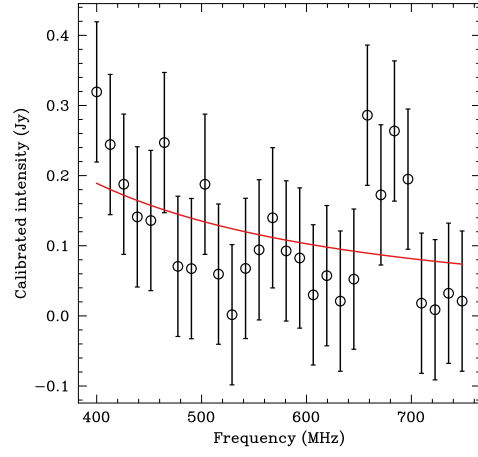
E.F., I.S., S.C., S.M.R. are members of the NANOGrav Physics Frontiers Center, supported by the NSF award 2020265.

A.P.C. is a Vanier Canada Graduate Scholar.

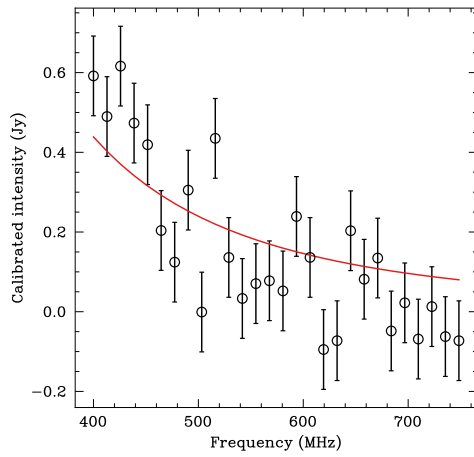
Appendix



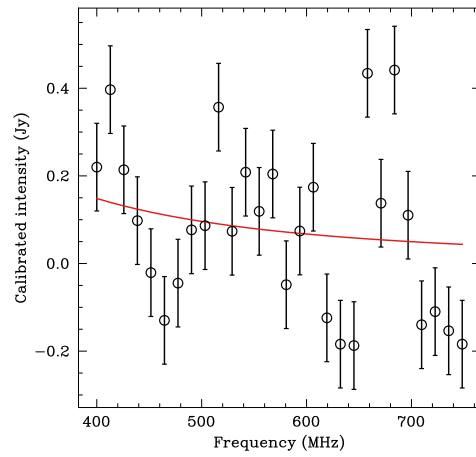
(a) 59341A



(b) 59341B

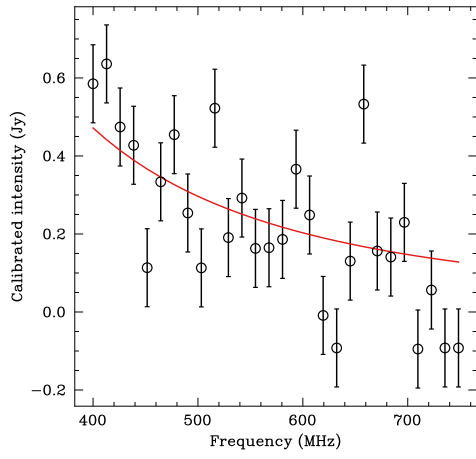


(c) 59456A

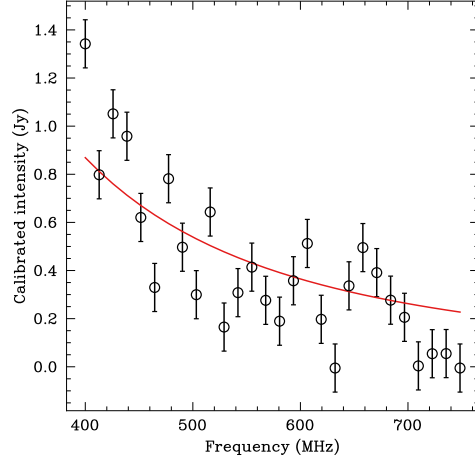


(d) 59456B

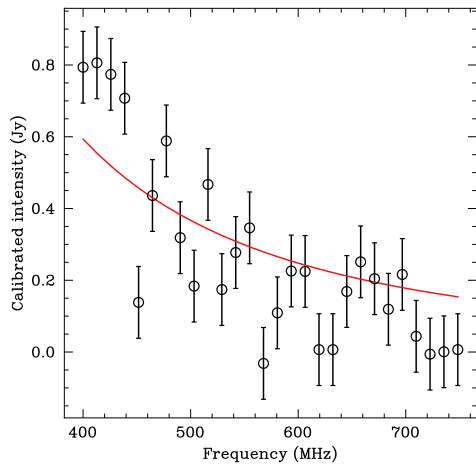
Fig. 1: The calibrated spectral fit of all bursts with intensity data.



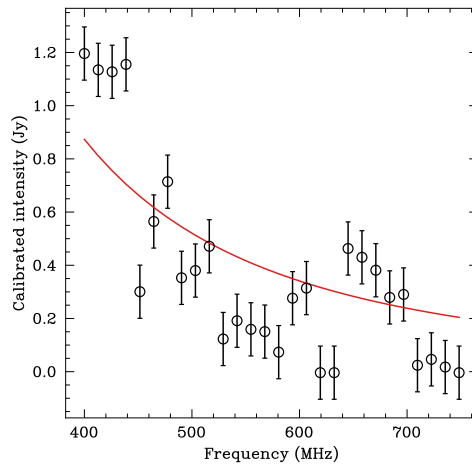
(e) 59460A



(f) 59463A

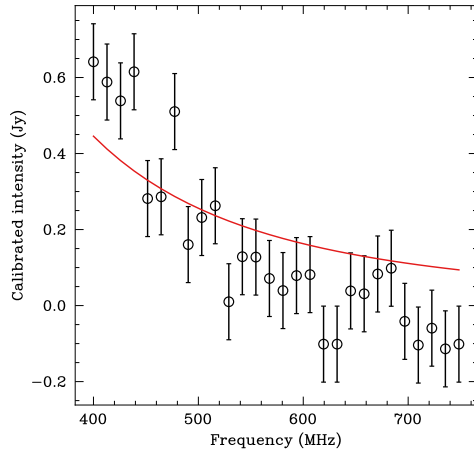


(g) 59548A

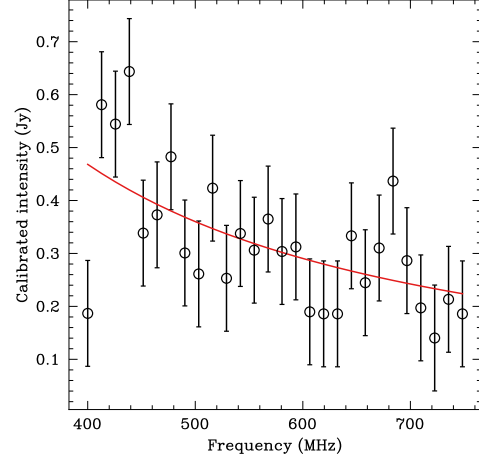


(h) 59553A

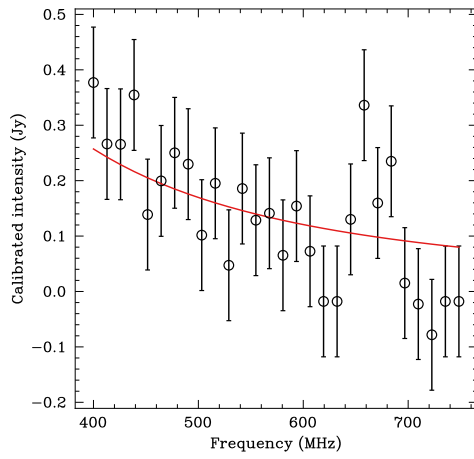
Fig. 1: Continued



(i) 59563A



(j) 59565A



(k) 59574A

Fig. 1: Continued

References

- [1] Hurley-Walker, N. *et al.* A radio transient with unusually slow periodic emission. *Nature* **601**, 526–530 (2022).
- [2] Hurley-Walker, N. *et al.* A long-period radio transient active for three decades. *Nature* **619**, 487–490 (2023).
- [3] Caleb, M. *et al.* An emission-state-switching radio transient with a 54-minute period. *Nature Astronomy* (2024).
- [4] Caleb, M. *et al.* Discovery of a radio-emitting neutron star with an ultra-long spin period of 76 s. *Nature Astronomy* **6**, 828–836 (2022).
- [5] Chen, K. & Ruderman, M. Pulsar Death Lines and Death Valley. *Astrophysical Journal* **402**, 264 (1993).
- [6] Zhang, B., Harding, A. K. & Muslimov, A. G. Radio Pulsar Death Line Revisited: Is PSR J2144-3933 Anomalous? *Astrophysical Journal Letters* **531**, L135–L138 (2000).
- [7] Philippov, A., Timokhin, A. & Spitkovsky, A. Origin of Pulsar Radio Emission. *Physical Review Letters* **124**, 245101 (2020).
- [8] Melrose, D. B. Coherent Radio Emission from Pulsars. *Philosophical Transactions of the Royal Society of London Series A* **341**, 105–115 (1992).
- [9] Mitra, D. Nature of Coherent Radio Emission from Pulsars. *Journal of Astrophysics and Astronomy* **38**, 52 (2017).
- [10] Kaspi, V. M. & Beloborodov, A. M. Magnetars. *Annual Review of Astronomy and Astrophysics* **55**, 261–301 (2017).
- [11] Popov, S. B. The Zoo of Isolated Neutron Stars. *Universe* **9**, 273 (2023).
- [12] Dib, R., Kaspi, V. M. & Gavriil, F. P. Rossi X-Ray Timing Explorer Monitoring of the Anomalous X-ray Pulsar 1E 1048.1 - 5937: Long-term Variability and the 2007 March Event. *Astrophysical Journal* **702**, 614–630 (2009).
- [13] Archibald, R. F. *et al.* Repeated, Delayed Torque Variations Following X-Ray Flux Enhancements in the Magnetar 1E 1048.1-5937. *Astrophysical Journal* **800**, 33 (2015).
- [14] Beniamini, P. *et al.* Evidence for an abundant old population of Galactic ultra-long period magnetars and implications for fast radio bursts. *The Monthly Notices of The Royal Astronomical Society* **520**, 1872–1894 (2023).
- [15] Caleb, M. *et al.* Radio and X-ray observations of giant pulses from XTE J1810

- 197. *The Monthly Notices of The Royal Astronomical Society* **510**, 1996–2010 (2022).
- [16] Maan, Y., Joshi, B. C., Surnis, M. P., Bagchi, M. & Manoharan, P. K. Distinct Properties of the Radio Burst Emission from the Magnetar XTE J1810-197. *Astrophysical Journal Letters* **882**, L9 (2019).
- [17] Tan, C. M. *et al.* LOFAR Discovery of a 23.5 s Radio Pulsar. *Astrophysical Journal* **866**, 54 (2018).
- [18] De Luca, A., Caraveo, P. A., Mereghetti, S., Tiengo, A. & Bignami, G. F. A Long-Period, Violently Variable X-ray Source in a Young Supernova Remnant. *Science* **313**, 814–817 (2006).
- [19] Gotthelf, E. V., Petre, R. & Hwang, U. The Nature of the Radio-quiet Compact X-Ray Source in Supernova Remnant RCW 103. *Astrophysical Journal Letters* **487**, L175–L179 (1997).
- [20] D’Ài, A. *et al.* Evidence for the magnetar nature of 1E 161348-5055 in RCW 103. *The Monthly Notices of The Royal Astronomical Society* **463**, 2394–2404 (2016).
- [21] Pelisoli, I. *et al.* A survey for radio emission from white dwarfs in the VLA Sky Survey. *The Monthly Notices of The Royal Astronomical Society* **531**, 1805–1822 (2024).
- [22] Marsh, T. R. *et al.* A radio-pulsing white dwarf binary star. *Nature* **537**, 374–377 (2016).
- [23] Pelisoli, I. *et al.* A 5.3-min-period pulsing white dwarf in a binary detected from radio to X-rays. *Nature Astronomy* **7**, 931–942 (2023).
- [24] Dong, F. A. *et al.* The second set of pulsar discoveries by CHIME/FRB/Pulsar: 14 rotating radio transients and 7 pulsars. *The Monthly Notices of The Royal Astronomical Society* **524**, 5132–5147 (2023).
- [25] CHIME Collaboration *et al.* An Overview of CHIME, the Canadian Hydrogen Intensity Mapping Experiment. *Astrophysical Journal Supplement* **261**, 29 (2022).
- [26] CHIME/FRB Collaboration *et al.* The CHIME Fast Radio Burst Project: System Overview. *Astrophysical Journal* **863**, 48 (2018).
- [27] CHIME/Pulsar Collaboration *et al.* The CHIME Pulsar Project: System Overview. *Astrophysical Journal Supplement* **255**, 5 (2021).
- [28] CHIME/FRB Collaboration *et al.* The First CHIME/FRB Fast Radio Burst Catalog. *Astrophysical Journal Supplement* **257**, 59 (2021).

- [29] Edwards, R. T., Hobbs, G. B. & Manchester, R. N. TEMPO2, a new pulsar timing package - II. The timing model and precision estimates. *The Monthly Notices of The Royal Astronomical Society* **372**, 1549–1574 (2006).
- [30] Luo, J. *et al.* PINT: A Modern Software Package for Pulsar Timing. *Astrophysical Journal* **911**, 45 (2021).
- [31] Klus, H., Ho, W. C. G., Coe, M. J., Corbet, R. H. D. & Townsend, L. J. Spin period change and the magnetic fields of neutron stars in Be X-ray binaries in the Small Magellanic Cloud. *The Monthly Notices of The Royal Astronomical Society* **437**, 3863–3882 (2014).
- [32] Cordes, J. M. & Lazio, T. J. W. NE2001.I. A New Model for the Galactic Distribution of Free Electrons and its Fluctuations. *arXiv e-prints* astro-ph/0207156 (2002).
- [33] Yao, J. M., Manchester, R. N. & Wang, N. A New Electron-density Model for Estimation of Pulsar and FRB Distances. *Astrophysical Journal* **835**, 29 (2017).
- [34] Price, D. C., Flynn, C. & Deller, A. A comparison of Galactic electron density models using PyGEDM. *Publications of the Astronomical Society of Australia* **38**, e038 (2021).
- [35] Chatterjee, S. *et al.* Precision Astrometry with the Very Long Baseline Array: Parallaxes and Proper Motions for 14 Pulsars. *Astrophysical Journal* **698**, 250–265 (2009).
- [36] Ruderman, M. A. & Sutherland, P. G. Theory of pulsars: polar gaps, sparks, and coherent microwave radiation. *Astrophysical Journal* **196**, 51–72 (1975).
- [37] Highland, V. L. ESTIMATION OF UPPER LIMITS FROM EXPERIMENTAL DATA (1986).
- [38] Rea, N. *et al.* Long-period Radio Pulsars: Population Study in the Neutron Star and White Dwarf Rotating Dipole Scenarios. *Astrophysical Journal* **961**, 214 (2024).
- [39] Buckley, D. A. H., Meintjes, P. J., Potter, S. B., Marsh, T. R. & Gänsicke, B. T. Polarimetric evidence of a white dwarf pulsar in the binary system AR Scorpii. *Nature Astronomy* **1**, 0029 (2017).
- [40] Mitra, D., Arjunwadkar, M. & Rankin, J. M. Polarized Quasiperiodic Structures in Pulsar Radio Emission Reflect Temporal Modulations of Non-stationary Plasma Flow. *Astrophysical Journal* **806**, 236 (2015).
- [41] Kramer, M., Liu, K., Desvignes, G., Karuppusamy, R. & Stappers, B. W. Quasi-periodic sub-pulse structure as a unifying feature for radio-emitting neutron stars.

Nature Astronomy **8**, 230–240 (2024).

- [42] Kisaka, S. & Tanaka, S. J. Efficiency of Synchrotron Radiation from Rotation-powered Pulsars. *Astrophysical Journal* **837**, 76 (2017).
- [43] Íñiguez-Pascual, D., Viganò, D. & Torres, D. F. Synchro-curvature emitting regions in high-energy pulsar models. *The Monthly Notices of The Royal Astronomical Society* **516**, 2475–2485 (2022).
- [44] Romani, R. W. Gamma-Ray Pulsars: Radiation Processes in the Outer Magnetosphere. *Astrophysical Journal* **470**, 469 (1996).
- [45] Cheng, K. S., Taam, R. E. & Wang, W. Pulsar Wind Nebulae and the X-Ray Emission of Nonaccreting Neutron Stars. *Astrophysical Journal* **617**, 480–489 (2004).
- [46] Potekhin, A. Y., De Luca, A. & Pons, J. A. Neutron Stars—Thermal Emitters. *Space science reviews* **191**, 171–206 (2015).
- [47] Kaplan, D. L. Yuan, Y.-F., Li, X.-D. & Lai, D. (eds) *Nearby, Thermally Emitting Neutron Stars*. (eds Yuan, Y.-F., Li, X.-D. & Lai, D.) *Astrophysics of Compact Objects*, Vol. 968 of *American Institute of Physics Conference Series*, 129–136 (AIP, 2008). [0801.1143](#).
- [48] Bahcall, J. N. & Wolf, R. A. An Observational Test of Theories of Neutron-Star Cooling. *Astrophysical Journal* **142**, 1254–1256 (1965).
- [49] McAlister, H. A. *et al.* First Results from the CHARA Array. I. An Interferometric and Spectroscopic Study of the Fast Rotator α Leonis (Regulus). *Astrophysical Journal* **628**, 439–452 (2005).
- [50] Petit, P., Böhm, T., Folsom, C. P., Lignières, F. & Cang, T. A decade-long magnetic monitoring of Vega. *Astronomy and Astrophysics* **666**, A20 (2022).
- [51] Dufton, P. L. *et al.* The VLT-FLAMES Tarantula Survey: The Fastest Rotating O-type Star and Shortest Period LMC Pulsar—Remnants of a Supernova Disrupted Binary? *Astrophysical Journal Letters* **743**, L22 (2011).
- [52] Lyubarsky, Y. Fast Radio Bursts from Reconnection in a Magnetar Magnetosphere. *Astrophysical Journal* **897**, 1 (2020).
- [53] Gil, J., Lyubarsky, Y. & Melikidze, G. I. Curvature Radiation in Pulsar Magnetospheric Plasma. *Astrophysical Journal* **600**, 872–882 (2004).
- [54] Camilo, F. *et al.* Revival of the Magnetar PSR J1622-4950: Observations with MeerKAT, Parkes, XMM-Newton, Swift, Chandra, and NuSTAR. *Astrophysical Journal* **856**, 180 (2018).

- [55] Giri, U. *et al.* Comprehensive Bayesian analysis of FRB-like bursts from SGR 1935+2154 observed by CHIME/FRB. *arXiv e-prints* arXiv:2310.16932 (2023).
- [56] Katz, J. I. GLEAM-X J162759.5–523504.3 as a white dwarf pulsar. *Astrophysics and Space Science* **367**, 108 (2022).
- [57] Tong, H. Discussions on the Nature of GLEAM-X J162759.5-523504.3. *Astrophysical Journal* **943**, 3 (2023).
- [58] Ravi, V. *et al.* Observations of radio pulses from CU Virginis. *The Monthly Notices of The Royal Astronomical Society* **408**, L99–L103 (2010).
- [59] Hyman, S. D., Lazio, T. J. W., Kassim, N. E. & Bartleson, A. L. Low-Frequency Radio Transients in the Galactic Center. *Astronomical Journal* **123**, 1497–1501 (2002).
- [60] Hyman, S. D. *et al.* GCRT J1742-3001: A New Radio Transient Toward the Galactic Center. *Astrophysical Journal* **696**, 280–286 (2009).
- [61] Tannock, M. E. *et al.* Weather on Other Worlds. V. The Three Most Rapidly Rotating Ultra-cool Dwarfs. *Astronomical Journal* **161**, 224 (2021).
- [62] Lorimer, D. R. & Kramer, M. *Handbook of Pulsar Astronomy* Vol. 4 (2004).
- [63] Gentile Fusillo, N. P. *et al.* A catalogue of white dwarfs in Gaia EDR3. *The Monthly Notices of The Royal Astronomical Society* **508**, 3877–3896 (2021).
- [64] The CHIME/FRB Collaboration *et al.* Updating the first CHIME/FRB catalog of fast radio bursts with baseband data. *arXiv e-prints* arXiv:2311.00111 (2023).
- [65] Beniamini, P., Hotokezaka, K., van der Horst, A. & Kouveliotou, C. Formation rates and evolution histories of magnetars. *The Monthly Notices of The Royal Astronomical Society* **487**, 1426–1438 (2019).
- [66] Beniamini, P., Wadiasingh, Z. & Metzger, B. D. Periodicity in recurrent fast radio bursts and the origin of ultralong period magnetars. *The Monthly Notices of The Royal Astronomical Society* **496**, 3390–3401 (2020).
- [67] Pearlman, A. B., Majid, W. A., Prince, T. A., Kocz, J. & Horiuchi, S. Pulse Morphology of the Galactic Center Magnetar PSR J1745-2900. *Astrophysical Journal* **866**, 160 (2018).
- [68] Camilo, F. *et al.* The Variable Radio-to-X-Ray Spectrum of the Magnetar XTE J1810-197. *Astrophysical Journal* **669**, 561–569 (2007).
- [69] Camilo, F., Ransom, S. M., Halpern, J. P. & Reynolds, J. 1E 1547.0-5408: A Radio-emitting Magnetar with a Rotation Period of 2 Seconds. *Astrophysical Journal Letters* **666**, L93–L96 (2007).

- [70] Levin, L. *et al.* A Radio-loud Magnetar in X-ray Quiescence. *Astrophysical Journal Letters* **721**, L33–L37 (2010).
- [71] Lazaridis, K. *et al.* Radio spectrum of the AXP J1810-197 and of its profile components. *The Monthly Notices of The Royal Astronomical Society* **390**, 839–846 (2008).
- [72] Maron, O., Kijak, J., Kramer, M. & Wielebinski, R. Pulsar spectra of radio emission. *Astronomy and Astrophysics, Supplement* **147**, 195–203 (2000).
- [73] Ransom, S. M. *New search techniques for binary pulsars*. Ph.D. thesis, Harvard University, Massachusetts (2001).
- [74] Pang, D., Goseva-Popstojanova, K., Devine, T. & McLaughlin, M. A novel single-pulse search approach to detection of dispersed radio pulses using clustering and supervised machine learning. *The Monthly Notices of The Royal Astronomical Society* **480**, 3302–3323 (2018).
- [75] Agarwal, D., Aggarwal, K., Burke-Spolaor, S., Lorimer, D. R. & Garver-Daniels, N. FETCH: A deep-learning based classifier for fast transient classification. *The Monthly Notices of The Royal Astronomical Society* **497**, 1661–1674 (2020).
- [76] Aggarwal, K. *et al.* Your: Your Unified Reader. *The Journal of Open Source Software* **5**, 2750 (2020).
- [77] Karako-Argaman, C. *et al.* Discovery and Follow-up of Rotating Radio Transients with the Green Bank and LOFAR Telescopes. *Astrophysical Journal* **809**, 67 (2015).
- [78] Good, D. C. *et al.* First Discovery of New Pulsars and RRATs with CHIME/FRB. *Astrophysical Journal* **922**, 43 (2021).
- [79] Remazeilles, M., Dickinson, C., Banday, A. J., Bigot-Sazy, M. A. & Ghosh, T. An improved source-subtracted and destriped 408-MHz all-sky map. *The Monthly Notices of The Royal Astronomical Society* **451**, 4311–4327 (2015).
- [80] Haslam, C. G. T., Salter, C. J., Stoffel, H. & Wilson, W. E. A 408-MHZ All-Sky Continuum Survey. II. The Atlas of Contour Maps. *Astronomy and Astrophysics, Supplement* **47**, 1 (1982).
- [81] Polisensky, E. *et al.* Exploring the Transient Radio Sky with VLITE: Early Results. *Astrophysical Journal* **832**, 60 (2016).
- [82] Clarke, T. E. *et al.* Hall, H. J., Gilmozzi, R. & Marshall, H. K. (eds) *Commensal low frequency observing on the NRAO VLA: VLITE status and future plans*. (eds Hall, H. J., Gilmozzi, R. & Marshall, H. K.) *Ground-based and Airborne Telescopes VI*, Vol. 9906 of *Society of Photo-Optical Instrumentation Engineers*

(*SPIE*) *Conference Series*, 99065B (2016).

- [83] Mohan, N. & Rafferty, D. PyBDSF: Python Blob Detection and Source Finder. *Astrophysics Source Code Library*, record ascl:1502.007 (2015). [1502.007](#).
- [84] Coppin, P. GRBweb [Online]. https://icecube.wisc.edu/~grbweb_public (2022).
- [85] Curtin, A. P. *et al.* Limits on Fast Radio Burst-like Counterparts to Gamma-Ray Bursts Using CHIME/FRB. *Astrophysical Journal* **954**, 154 (2023).